Engineering Analysis with Boundary Elements 115 (2020) 168–211

Contents lists available at ScienceDirect

Engineering Analysis with Boundary Elements

journal homepage: www.elsevier.com/locate/enganabound

A new error estimation technique for solving torsion bar problem with inclusion by using BEM

K.H. Chen [a], J.H. Kao [b,*], J.T. Chen [b,c,d,e,*], J.F. Liau [a]

[a] Department of Civil Engineering, National Ilan University, Ilan 26047, Taiwan
[b] Department of Harbor and River Engineering, National Taiwan Ocean University, Keelung 20224, Taiwan
[c] Department of Mechanical and Mechatronic Engineering, National Taiwan Ocean University, Keelung, 20224, Taiwan
[d] Department of Ocean Engineering and Technology, National Taiwan Ocean University, Keelung 20224, Taiwan
[e] Center of Excellence for Ocean Engineering, National Taiwan Ocean University, Keelung 20224, Taiwan

ARTICLE INFO

Keywords:
Error estimation technique
Boundary integral equation
Torsion bar
Inclusion
Auxiliary problem

ABSTRACT

In this paper, the torsion problem is analyzed by boundary element method (BEM). After applying a new error estimation technique in the BEM, we can derive the numerical error of BEM. We extend the research of previous literature by the authors Chen and Chen [1], to the real engineering problem. This paper estimates the discretizing error caused by using BEM for solving the torsion problem with inclusions. The main characteristic of this technique is that the exact solution is not known in prior. In the technique, we need to create an auxiliary problem that the government equation, domain shape, and boundary condition type are the same as the given real problem. Besides, it has an analytical solution that satisfies the governing equation. We can derive the suitable number of elements by solving the auxiliary problem. Subsequently, by using the suitable number of elements in the BEM, we can obtain the appropriate solution for the real problem. Finally, several cases in the literature are given to illustrate the validity of the novel approach applied in the BEM to solve the real problem.

1. Introduction

During the last decade, some themes of research focused on how to improve the numerical method. How to discrete the time domain is an important issue in the time-dependent problem. The finite difference scheme is a common method [2]. To improve the computer efficiency, researchers have developed the new discrete technique, such as Euler–Maruyama method [3], Crank-Nicolson scheme [4] et al. These methods have been successfully applied to solve the Boussinesq equation, the Cahn–Hilliard–Cook equation, the Swift–Hohenberg equation, the magnetohydrodynamics (MHD) equation et al. To solve the space domain problem, the common computational methods have Trefftz method and boundary element method. Although the exponential convergence of the approximation error with respect to the order of the approximating harmonic polynomial is proved in the Trefftz solution space, the accuracy of such the analytical solution may not be sufficient for some complex problems since Trefftz method is a type of domain method. A novel technique was proposed to expand a function to the local region which is named as the fast multipole expansion method. Recently, the conventional Trefftz method was extended to the multipole Trefftz method to treat with the large scale problem by introducing the multipole expansion to overcome the problem in the following reference [6]. Recent research on the local BIE, the local RBF and the local MFS can also solve complex problems. On the other hand, highly accurate collocation Trefftz method [5] is also one of the methods of improved accuracy. In this paper, Trefftz basis of Trefftz method is extended to estimate the numerical error of numerical method. We introduce the Trefftz basis as a quasi-analytical solution to substitute for the analytical solution of real problem.

Discretizing in boundary integral equation is a main process of the BEM for solving engineering problems [7–13]. When we transform a continuous system into a discrete system with a finite number of degrees of freedom, it would result in errors. In general, the discretizing error is defined by the difference between the analytical solution and the numerical result. The analytical solution of real problems is difficult to be obtained by mathematical formulation. There is no criterion in the choice of how many elements to derive one sufficiently accurate numerical solution. Sometimes, we can obtain a precise numerical result, and sometimes we can obtain the poor result when we choose a specified number of elements. Thus, estimation of discretizing error in the BEM is a key study.

There are very large quantities of studies in applying the hypersingular equation to find the residual as the error estimator [1,10]. In the literature [1,10], various versions of integral equations can be employed to

* Corresponding authors.
E-mail addresses: khc6177@niu.edu.tw (K.H. Chen), m93520009@mail.ntou.edu.tw (J.H. Kao), jtchen@mail.ntou.edu.tw (J.T. Chen).

https://doi.org/10.1016/j.enganabound.2020.02.012
Received 17 October 2019; Received in revised form 17 January 2020; Accepted 25 February 2020

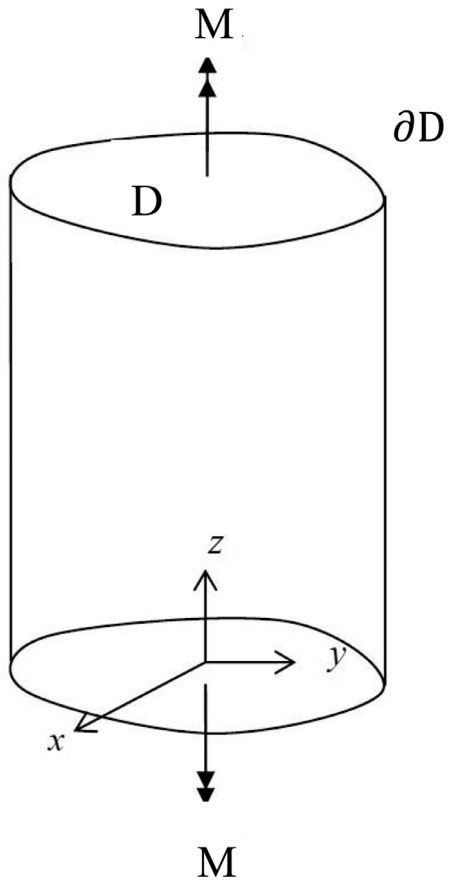

Fig. 1. Sketch of the torsion problem.

obtain the residual in discretizing process, accordingly both the strongly singular integral equation and hypersingular integral equation can independently resolve the unknown boundary data. The residuals derived by these two equations can be employed as indexes of estimating error. This provides a criterion for remeshing. Unfortunately, the index cannot be compared for different number of meshes because it is a pointwise error which depends on the number of meshes. The error trends can only be recognized by the derived index, but the index does not present the error magnitude. By using the new error estimation technique, we need to present an objective guideline to compare the error quantities in a different number of meshes.

2. Problem statement

Saint-Venant torsion problem of solid mechanics is very important topic; it can be described by using warping function, conjugate warping function or the stress function. Early related research has Muskhelishvili(1953) [14], Sapountzakis and Mokos (2003) [15] and Timoshenko and Gooder (1970) [16], and so on. Following the approach of Saint-Venant torsion problem [15], the displacement field can be assumed as

$$u_x \equiv u = -\theta yz \tag{1}$$

$$u_y \equiv v = \theta zx \tag{2}$$

$$u_z \equiv w = \theta\varphi(x, y) \tag{3}$$

where θ is the angle of twist per unit length along the z-direction and φ is the warping function. The coordinate system is depicted in Fig. 1. The relation of strain and displacement is satisfied with the generalized Hook's law and can be found in the common elasticity book as shown below:

$$\varepsilon_x = \frac{\partial u}{\partial x}, \tag{4}$$

$$\varepsilon_y = \frac{\partial u}{\partial y}, \tag{5}$$

$$\varepsilon_z = \frac{\partial u}{\partial z}, \tag{6}$$

$$\gamma_{xy} = \frac{\partial u}{\partial y} + \frac{\partial v}{\partial x}, \tag{7}$$

$$\gamma_{yz} = \frac{\partial v}{\partial z} + \frac{\partial w}{\partial y}, \tag{8}$$

$$\gamma_{zx} = \frac{\partial w}{\partial x} + \frac{\partial u}{\partial z}. \tag{9}$$

After substituting the displacement of Eqs. (1)–(3) into Eqs. (4)–(6) and Eqs. (7)–(9), we obtain the strain components as follows:

$$\varepsilon_x = \varepsilon_y = \varepsilon_z = \gamma_{xy} = 0, \tag{10}$$

$$\gamma_{xz} = \theta\left(\frac{\partial\varphi}{\partial x} - y\right), \tag{11}$$

$$\gamma_{yz} = \theta\left(\frac{\partial\varphi}{\partial y} + x\right) \tag{12}$$

By applying the generalized Hook's law, we obtain the stress field

$$\tau_x = \tau_y = \tau_z = \tau_{xy} = 0 \tag{13}$$

$$\tau_{xz} = \mu\theta\left(\frac{\partial\varphi}{\partial x} - y\right), \tag{14}$$

$$\tau_{yz} = \mu\theta\left(\frac{\partial\varphi}{\partial y} + x\right). \tag{15}$$

where μ is the shear modulus. There is no distortion in the planes of cross-sections since Eq. (10). We have the state of pure shear at each point defined by the stress components τ_{xz} and τ_{yz}. The force equilibrium equation is shown below:

$$\frac{\partial\tau_x}{\partial x} + \frac{\partial\tau_{xy}}{\partial y} + \frac{\partial\tau_{xz}}{\partial z} + F_x = 0 \tag{16}$$

$$\frac{\partial\tau_y}{\partial y} + \frac{\partial\tau_{xy}}{\partial x} + \frac{\partial\tau_{yz}}{\partial z} + F_y = 0 \tag{17}$$

$$\frac{\partial\tau_z}{\partial z} + \frac{\partial\tau_{xz}}{\partial x} + \frac{\partial\tau_{yz}}{\partial y} + F_z = 0 \tag{18}$$

Substituting Eqs. (13)–(15) into Eqs. (16)-(18), we can obtain the warping function,φ, which satisfies the Laplace equation as

$$\frac{\partial^2\varphi}{\partial x^2} + \frac{\partial^2\varphi}{\partial y^2} = 0, \quad (x, y) \text{ in domain D}, \tag{19}$$

On the cylindrical surface, the stress in Eqs. (13)–(15) results in zero traction of $t_x = t_y = t_z = 0$, where t_x, t_y, and t_z are the traction in x, y, and z-direction. By substituting the normal vector, t_z becomes

$$t_z = \tau_{zx}n_x + \tau_{zy}n_y, \quad (x, y) \text{ on } B_0 \tag{20}$$

Substitution of Eqs. (14) and (15) into Eq. (20), we have

$$\frac{\partial\varphi}{\partial x}n_x + \frac{\partial\varphi}{\partial y}n_y = \nabla\varphi\cdot n = \frac{\partial\varphi}{\partial n} = yn_x - xn_y, (x, y) \text{ on } B_0 \tag{21}$$

while the cross-section of a bar with holes and/or inclusions is shown in Fig. 2, the ideal boundary condition (BC) between the matrix and holes/inclusions satisfies with the continuity conditions for the displacement and the equilibrium condition for traction [17,18] as follows

$$\varphi^{Mr} = \varphi^I, (x, y) \text{ on } B_i, i = 1, 2, 3, \ldots. \tag{22}$$

$$\mu_0\frac{\partial\varphi_i^{Mr}}{\partial n} - \mu_i\frac{\partial\varphi_i^I}{\partial n} = (\mu_0 - \mu_i)(yn_x - xn_y), (x, y) \text{ on } Bi, \mathrm{i} = 1, 2, 3, \ldots. \tag{23}$$

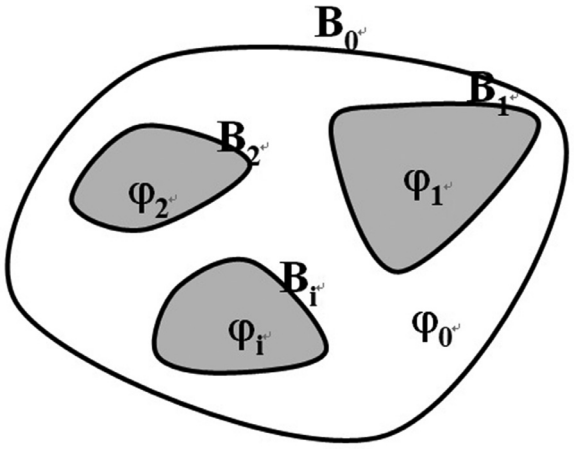

Fig. 2. Sketch of cross section of the bar with inclusions for torsion problem.

where n_x and n_y are the x and y components of the outward unit normal n on the boundary B_i, $\partial\varphi/\partial n$ is the normal derivative, the superscripts "*Mr*" and "*I*" denote the matrix and inclusion, respectively, B_i is the ith interface boundary,μ_0 is the shear modulus for matrix and μ_i is the shear modulus for the ith inclusion.

We can obtain the resultant moment applied at the end of the bar by solving the warping function. It is statically equivalent to the sum of the torsion couple of the system of stresses defined by Eqs. (13)–(15). The torsion rigidity G is [19]

$$\begin{aligned} G &= \mu \int_D \left(x^2 + y^2 + x\frac{\partial \varphi}{\partial y} - y\frac{\partial \varphi}{\partial x} \right) dD \\ &= \mu \int_D (x^2 + y^2) dD + \mu \int_D \left(x\frac{\partial \varphi}{\partial y} - y\frac{\partial \varphi}{\partial x} \right) dD \\ &= -\mu \oint_B \varphi (y n_x - x n_y) dB + \frac{\mu}{16} \oint_B \frac{\partial (x^2 + y^2)}{\partial n} dB \\ &= -\mu \oint_B \varphi \frac{\partial \varphi}{\partial n} dB + \frac{\mu}{16} \oint_B \frac{\partial (x^2 + y^2)}{\partial n} dB \end{aligned} \tag{24}$$

The total rigidity G containing matrix and inclusion domain is separated into

$$G = G^M + G^I \tag{25}$$

3. Boundary element method

The boundary integral equation for the domain point of Laplace problem can be derived from Green's third identity as:

$$2\pi u(x) = \int T(s,x) u(s) dB(s) - \int U(s,x) t(s) dB(s), x \in D \tag{26}$$

where $U(s, x)$ is the fundamental solution which satisfies:

$$\nabla^2 U(s,x) = 2\pi\delta(x - s) \tag{27}$$

in which $U(s, x) = \ln r$ and $\delta(x - s)$ is the Dirac-delta function. x and s are collocation and source points, respectively. $T(x, s)$ is defined by

$$T(s,x) = \frac{\partial U(s,x)}{\partial n_s} \tag{28}$$

where n_s is the out-normal direction at the boundary point s. By approaching the field point x to the boundary, the integral equation of the Eq. (26) can be rewritten as:

$$\pi u(x) = CPV \int_B T(s,x) u(s) dB(s) - RPV \int_B U(s,x) t(s) dB(s), x \in B \tag{29}$$

where *CPV* and *RPV* are the Cauchy principal value and Riemann principal value, respectively. The Eq. (29) is the singular integral formulation in the conventional BEM, we can call *UT* method. The linear algebraic system of Eq. (29) can be obtained by discretizing N number of constant boundary elements.

$$[U]\{t\} = [T]\{u\} \tag{30}$$

The problem in Fig. 2 can be decomposed into two parts by using the concept of domain decomposition. One is the torsion problem of a shaft with multiple holes and the other is a problem of each inclusion, each domain satisfies the Laplace equation. The linear algebraic system in the matrix can be obtained as:

$$\begin{bmatrix} T_{00}^{Mr} & \cdots & T_{0k}^{Mr} \\ \vdots & \ddots & \vdots \\ T_{k0}^{Mr} & \cdots & T_{kk}^{Mr} \end{bmatrix} \begin{Bmatrix} \varphi_0^{Mr} \\ \vdots \\ \varphi_k^{Mr} \end{Bmatrix} = \begin{bmatrix} U_{00}^{Mr} & \cdots & U_{0k}^{Mr} \\ \vdots & \ddots & \vdots \\ U_{k0}^{Mr} & \cdots & U_{kk}^{Mr} \end{bmatrix} \begin{Bmatrix} \frac{\partial \varphi_0^{Mr}}{\partial n} \\ \vdots \\ \frac{\partial \varphi_k^{Mr}}{\partial n} \end{Bmatrix} \tag{31}$$

where the superscripts "*Mr*" denote matrix, the first subscript, i (i = 1,2,…,k), in T_{ij}^{Mr} and U_{ij}^{Mr} denote the index of i^{th} hole/inclusion where the collocation point is located and the second subscript "j" (j = 1,2,…,k) denotes the j^{th} hole/inclusion when integrating on each boundary data $\{\varphi_j^{Mr}\}$ and $\{\frac{\partial \varphi_j^{Mr}}{\partial n}\}$, k is the number of inclusions embedded in the matrix. For each inclusion, we have

$$\begin{bmatrix} T_{00}^{I} & \cdots & T_{0k}^{I} \\ \vdots & \ddots & \vdots \\ T_{k0}^{I} & \cdots & T_{kk}^{I} \end{bmatrix} \begin{Bmatrix} \varphi_0^{I} \\ \vdots \\ \varphi_k^{I} \end{Bmatrix} = \begin{bmatrix} U_{00}^{I} & \cdots & U_{0k}^{I} \\ \vdots & \ddots & \vdots \\ U_{k0}^{I} & \cdots & U_{kk}^{I} \end{bmatrix} \begin{Bmatrix} \frac{\partial \varphi_0^{I}}{\partial n} \\ \vdots \\ \frac{\partial \varphi_k^{I}}{\partial n} \end{Bmatrix} \tag{32}$$

where the superscripts "*I*" denotes the inclusion. In order to satisfy the continuity conditions of displacement and equilibrium condition of traction on the interface in Eqs. (22) and (23), the arrangement matrix is given

$$\begin{aligned} &\begin{bmatrix} T_{00}^{Mr} & T_{01}^{Mr} & \cdots & T_{0k}^{Mr} & -\frac{\mu_1}{\mu_0} U_{01}^{Mr} & \cdots & -\frac{\mu_k}{\mu_0} U_{0k}^{Mr} \\ T_{10}^{Mr} & T_{11}^{Mr} & \cdots & T_{1k}^{Mr} & -\frac{\mu_1}{\mu_0} U_{11}^{Mr} & \cdots & -\frac{\mu_k}{\mu_0} U_{1k}^{Mr} \\ \vdots & \vdots & \ddots & \vdots & \vdots & \ddots & \vdots \\ T_{k0}^{Mr} & T_{k1}^{Mr} & \cdots & T_{kk}^{Mr} & -\frac{\mu_1}{\mu_0} U_{k1}^{Mr} & \cdots & -\frac{\mu_k}{\mu_0} U_{kk}^{Mr} \\ 0 & T_{11}^{I} & \cdots & T_{1k}^{I} & -U_{11}^{I} & \cdots & -U_{1k}^{I} \\ \vdots & \vdots & \ddots & \vdots & \vdots & \ddots & \vdots \\ \vdots & T_{k1}^{I} & \cdots & T_{kk}^{I} & -U_{k1}^{I} & \cdots & -U_{kk}^{I} \end{bmatrix} \begin{Bmatrix} \varphi_0^{Mr} \\ \varphi_1^{Mr} \\ \vdots \\ \varphi_k^{Mr} \\ \frac{\partial \varphi_1^{I}}{\partial n} \\ \vdots \\ \frac{\partial \varphi_k^{I}}{\partial n} \end{Bmatrix} \\ &= \begin{bmatrix} U_{00}^{Mr} & U_{01}^{Mr} & \cdots & U_{0k}^{Mr} \\ U_{10}^{Mr} & U_{11}^{Mr} & \cdots & U_{1k}^{Mr} \\ \vdots & \vdots & \ddots & \vdots \\ U_{k0}^{Mr} & U_{k1}^{Mr} & \cdots & U_{kk}^{Mr} \end{bmatrix} \begin{Bmatrix} y n_x - x n_y \\ \frac{(\mu_0 - \mu_1)}{\mu_0} (y n_x - x n_y) \\ \vdots \\ \frac{(\mu_0 - \mu_k)}{\mu_0} (y n_x - x n_y) \end{Bmatrix} \end{aligned} \tag{33}$$

After solving the unknown vector, φ_i^I and $\frac{\partial \varphi_i^I}{\partial n}$, in Eq. (33), the torsional rigidity can be easily determined by Eqs. (24) and (25).

4. New error estimation technique [20]

By comparing the numerical solution with the analytical solution, we gain the error norm, however, in the realistic engineering problem it is not obtained easily. To overcome the drawback, an alternative problem is defined to substitute for the original problem. The domain shape and boundary condition type in the new specific problem are the same as the original problem. Furthermore, the exact solution to the auxiliary problem, similar to the exact solution of the original problem, can be easily derived by the aid of the set of complementary solutions.

Through simplification, analytical solutions can be obtained. By comparing numerical and analytical solutions, we can obtain the error norm. However, the analytical solution is not easily obtained in the real engineering problem. In this research, we will overcome this drawback through the defined alternative problem. The domain shape and

Table 1
T-complete set for Laplace equation.

Laplace equation			
G.E		$\nabla^2\varphi(x)=0$	
		Interior basis	Exterior basis
Basis function	1D	1, x	1, x
	2D	$\rho^n\cos(n\theta)$, $\rho^n\sin(n\theta)$ $n=0,1,2,\ldots$	$\rho^{-n}\cos(n\theta)$, $\rho^{-n}\sin(n\theta)$ $n=1,2,\ldots$
	3D	$\rho^m P_m^n\cos(\theta)\cos(n\theta)$ $\rho^m P_m^n\cos(\theta)\sin(n\theta)$ $n=0,1,2,\cdots$ $m=0,1,2,\cdots$	$\rho^{-(m+1)} P_m^n\cos(\theta)\cos(n\theta)$ $\rho^{-(m+1)} P_m^n\cos(\theta)\sin(n\theta)$ $n=0,1,2,\cdots$ $m=0,1,2,\cdots$

boundary condition type in the alternative problem are the same as the original problem. Furthermore, we can easily derive the exact solution in the alternative problem, this exact solution approximates the analytical solution of the original problem. We call alternative problem is the auxiliary problem.

4.1. Defining the G.E., contour and B.C. type

In the auxiliary problem, we set the governing equation, geometry contour and the boundary condition type to be the same as the original problem.

4.2. Constructing the exact solution

The exact solution, $\varphi^q(x)$, in the auxiliary problem at an arbitrary point x in the domain is the linear combination of the set functions as follows:

$$\varphi^q(x)=\sum_{j=1}^{M} v_j\Omega_j(x), x\in D \tag{34}$$

where the $\Omega_j(x)$ is chosen by the T-complete set functions which satisfy the G.E., M is the total number of the complementary solutions and V_j denotes the undetermined coefficient. T-complete sets are represented in Table 1 for the Laplace equation. Each of the function $\Omega_j(x)$ of T-complete set functions satisfies the G.E. as:

$$\nabla^2\Omega_j(x)=0, j=1,\ldots,M \tag{35}$$

Because of the linear property of the differential operator in G.E., the potential, $\varphi_j^q(x)$, satisfies the G.E. as:

$$\nabla^2\varphi^q(x)=\sum_{j=1}^{M} v_j\nabla^2\Omega_j=0 \tag{36}$$

4.3. Specifying B.C

The boundary-value in the auxiliary problem at the N number of collocation points is specified with the B.C. in the original problem. The boundary condition of the auxiliary problem is the same as the original problem. The undetermined coefficient, v_j, can be determined by matching the B.C. of the real problem. Therefore, the exact solution of the auxiliary problem is similar to the exact solution of the original problem. The two problems have the same boundary contour and B.C. type, and the B.C. of the auxiliary problem is given as:

$$\overline{\varphi}^q(x)=\sum_{j=1}^{M} v_j\Omega_j(x), x\in B_1 \tag{37}$$

the derivative of the normal direction (flux) is shown below:

$$\frac{\partial\overline{\varphi}^q(x)}{\partial n_x}=\sum_{j=1}^{M} v_j\frac{\partial\Omega_j(x)}{\partial n_x}=\sum_{j=1}^{M} v_j w_j(x), x\in B_2 \tag{38}$$

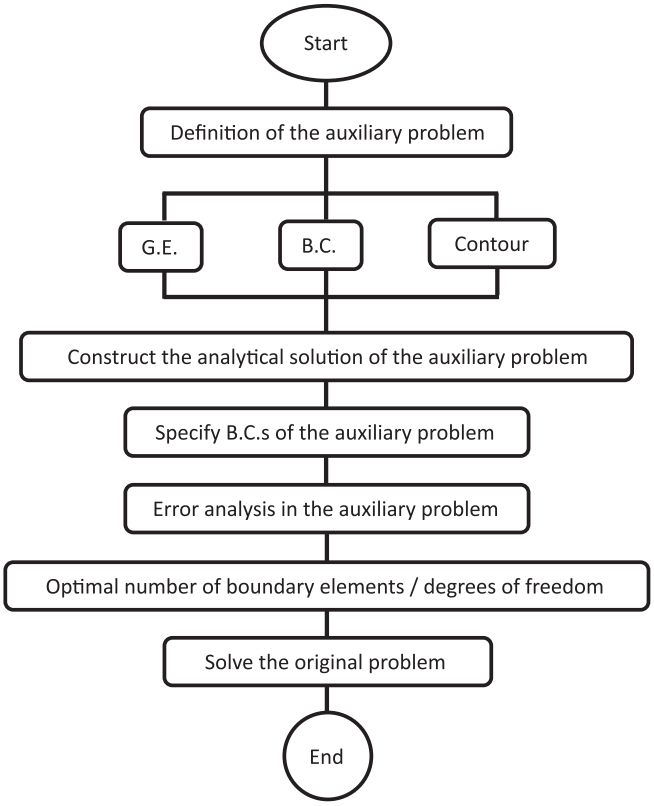

Fig. 3. Flowchart of the new error estimation technique.

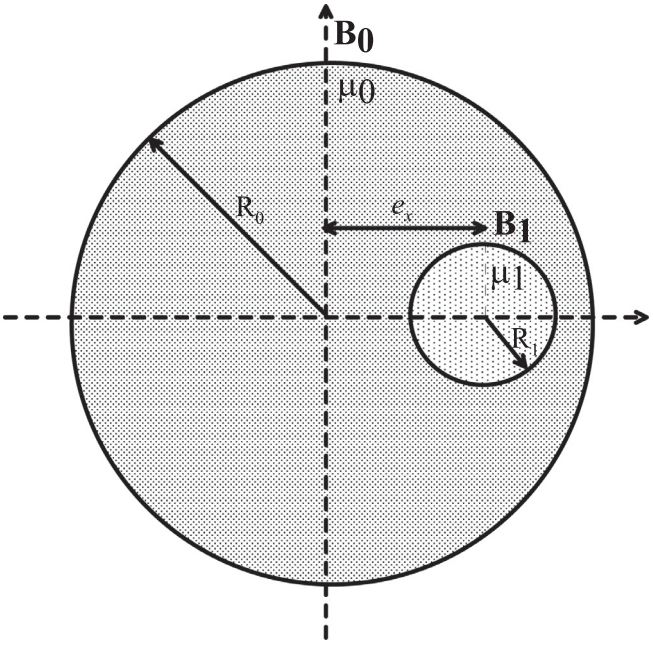

Fig. 4. Sketch of problem in the case 1.

where $\overline{\varphi}^q(x)$ and $\frac{\partial\overline{\varphi}^q(x)}{\partial n_x}$ are the known potential. The auxiliary problem can be solved by using the Trefftz method and the BEM. By comparing the numerical solution with the exact solution, we can obtain the error norm. Difference between the auxiliary problem and the original problem are formulated as follows:

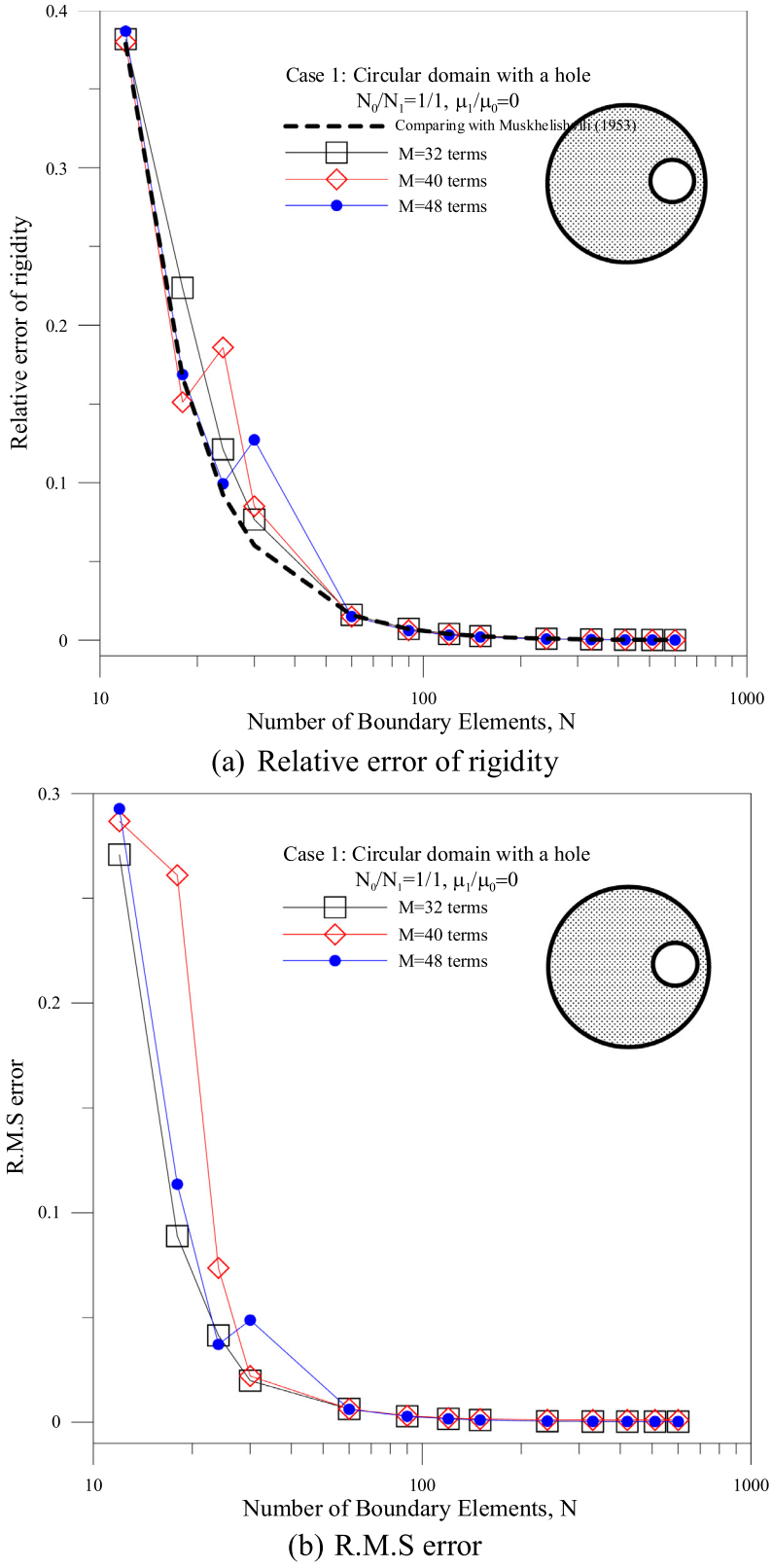

Fig. 5. The error analysis versus the number of boundary elements for the different terms of Trefftz basis in the case 1 ($\mu_1/\mu_0 = 0$).

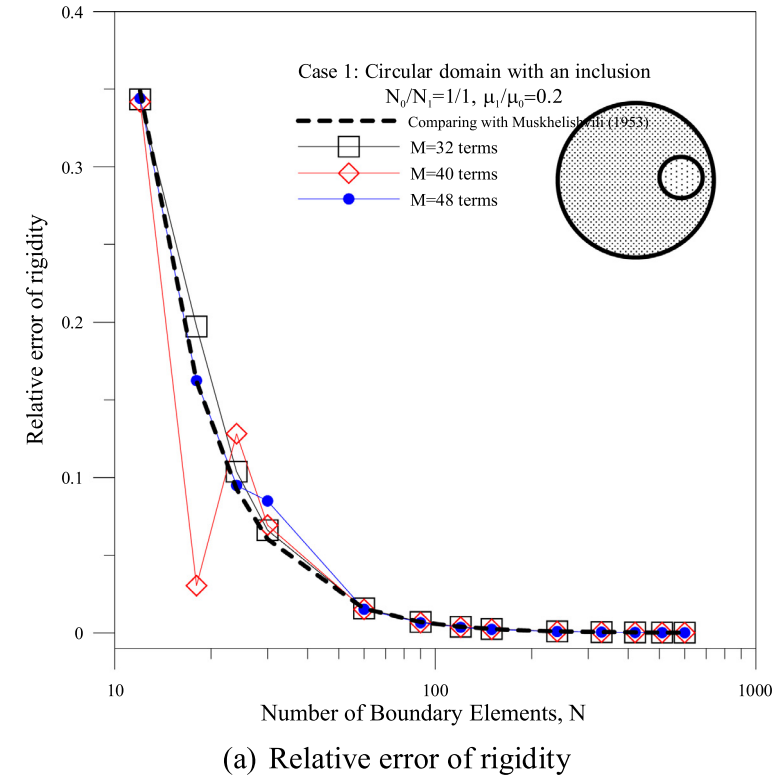

(a) Relative error of rigidity

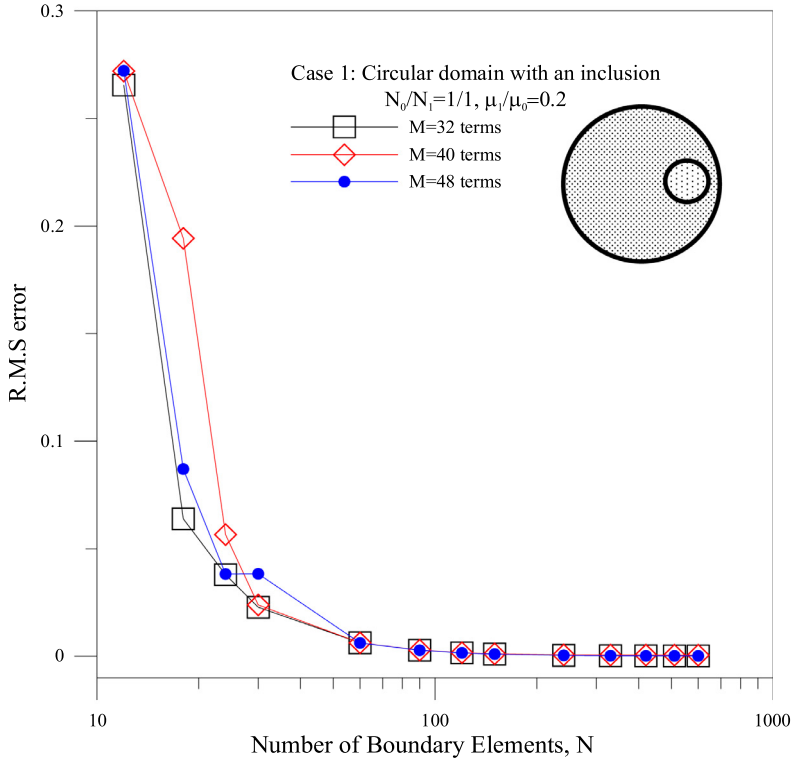

(b) R.M.S error

Fig. 6. The error analysis versus the number of boundary elements for the different terms of Trefftz basis in the case 1 ($\mu_1/\mu_0 = 0.2$).

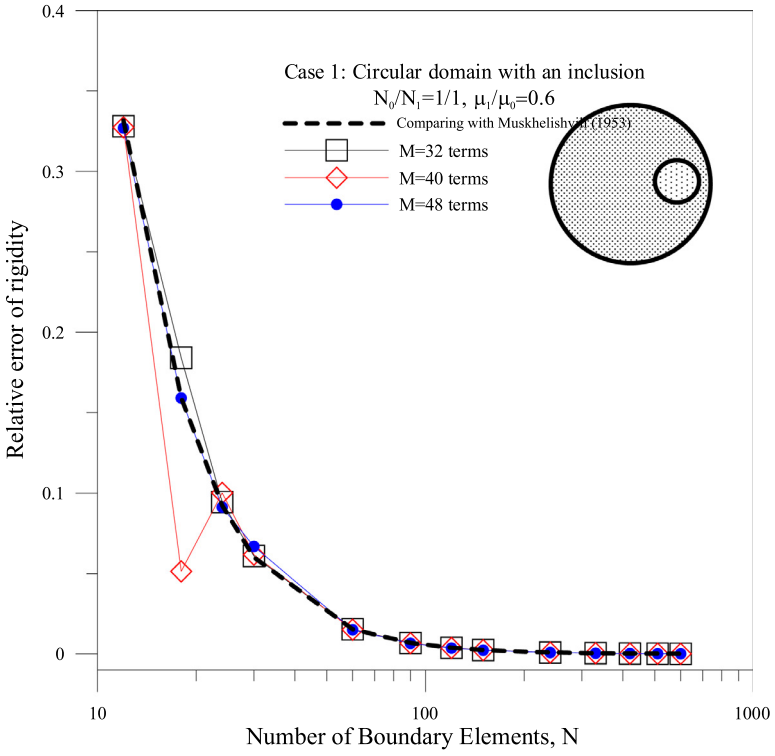

(a) Relative error of rigidity

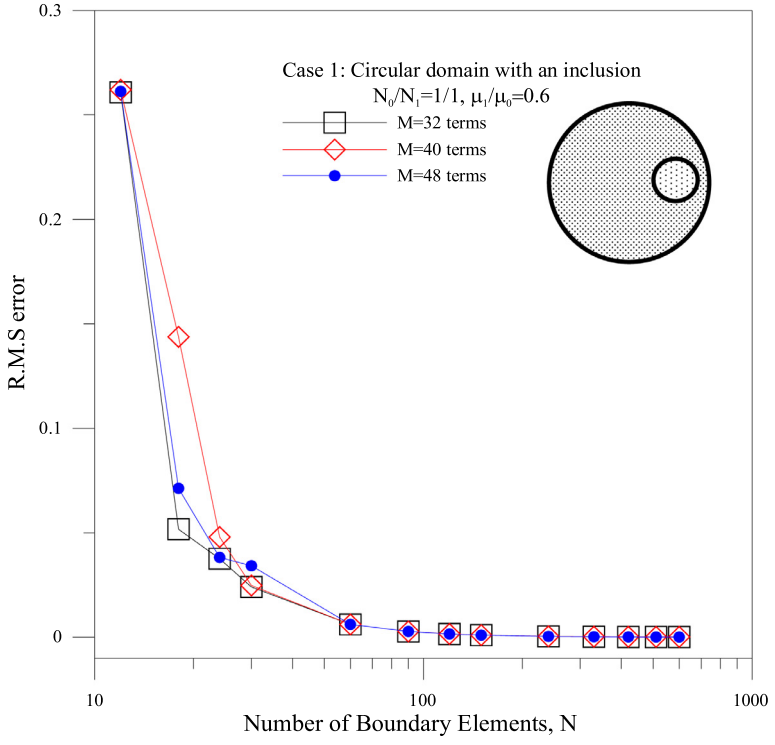

(b) R.M.S error

Fig. 7. The error analysis versus the number of boundary elements for the different terms of Trefftz basis in the case 1 ($\mu_1/\mu_0 = 0.6$).

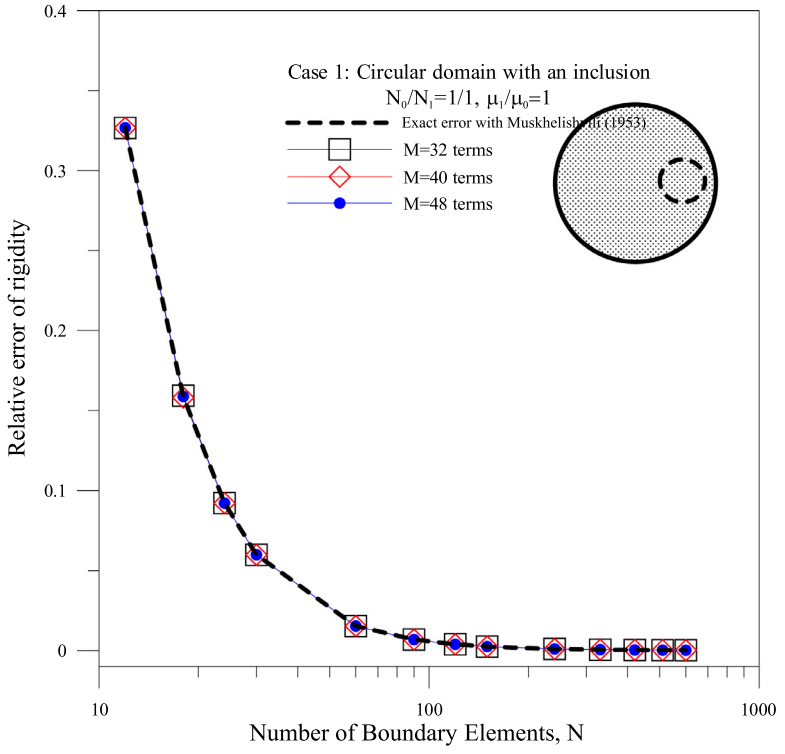

(a) Relative error of rigidity

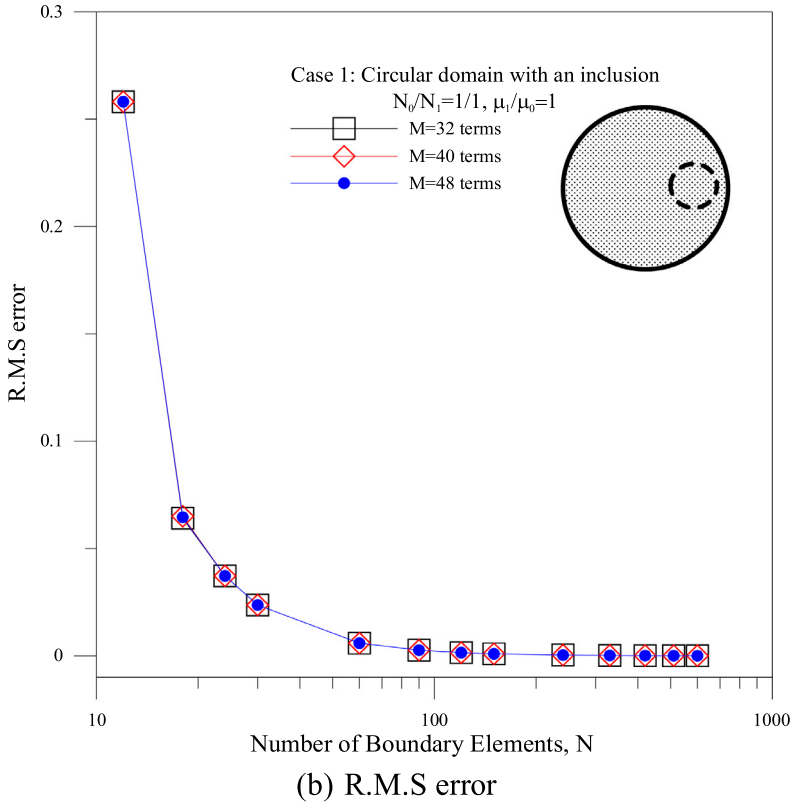

(b) R.M.S error

Fig. 8. The error analysis versus the number of boundary elements for the different terms of Trefftz basis in the case 1 ($\mu_1/\mu_0 = 1$).

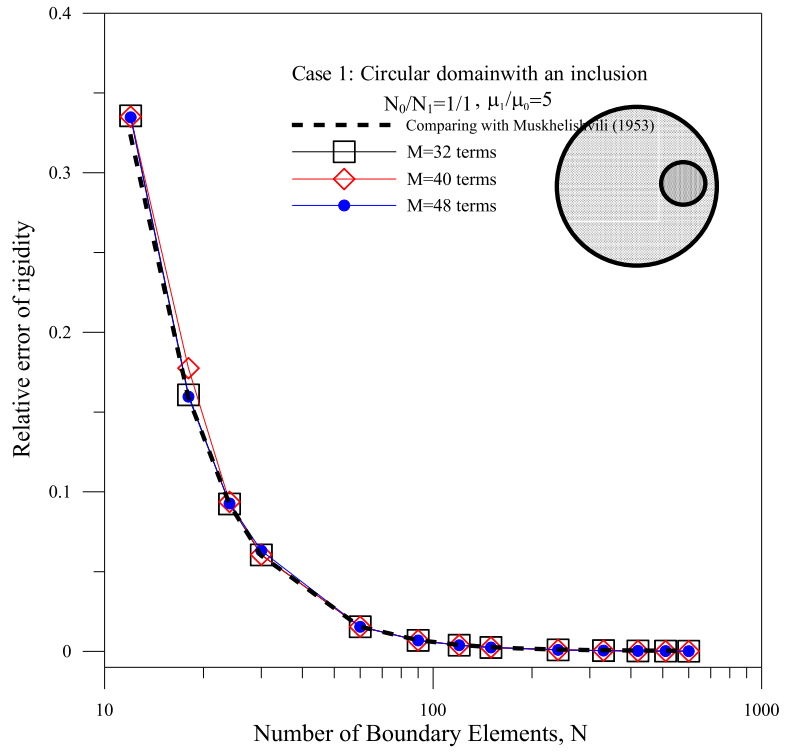

(a) Relative error of rigidity

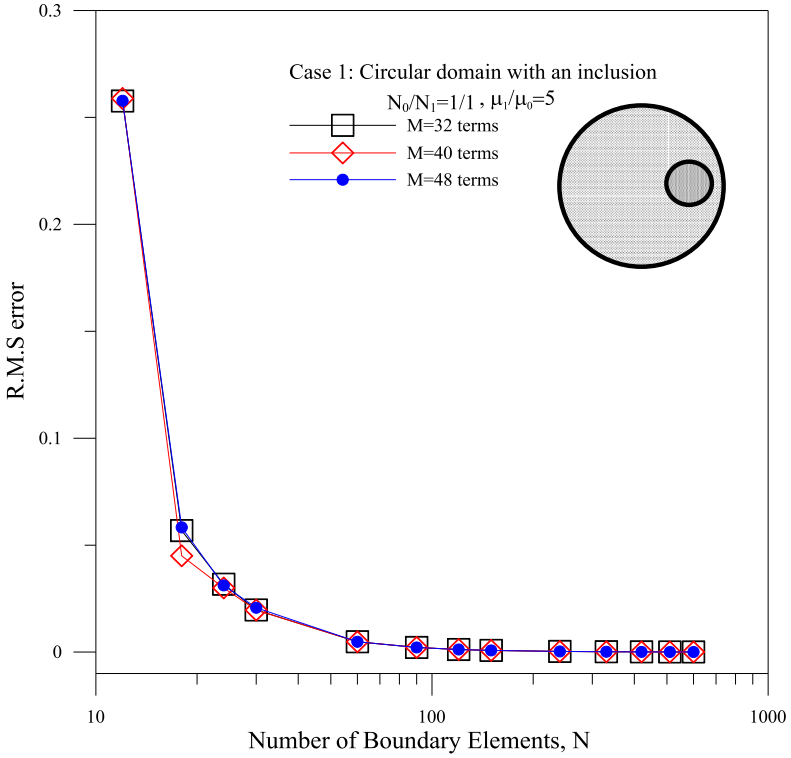

(b) R.M.S error

Fig. 9. The error analysis versus the number of boundary elements for the different terms of Trefftz basis in the case 1 ($\mu_1/\mu_0 = 5$).

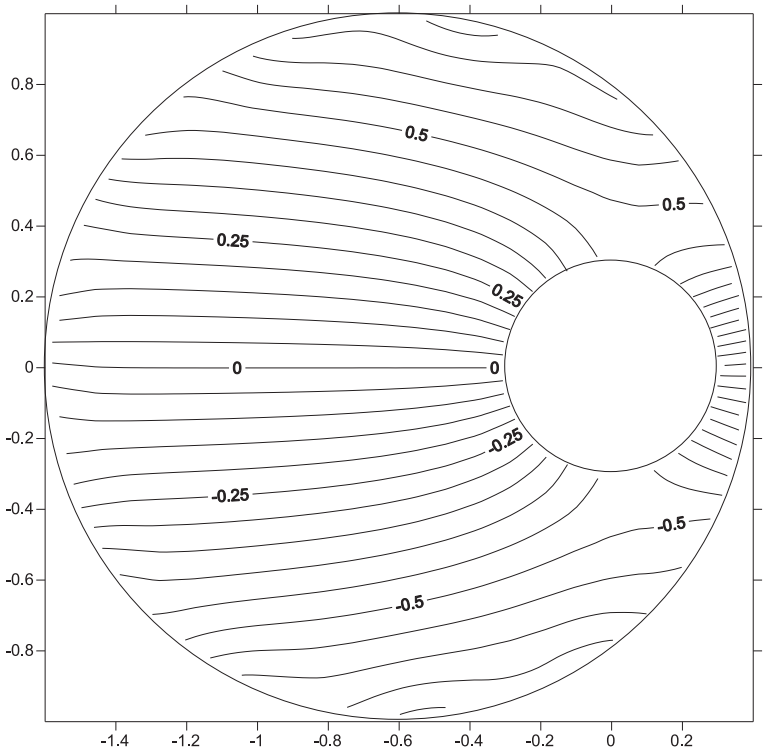

(a) Exact solution of the auxiliary problem (M=48)

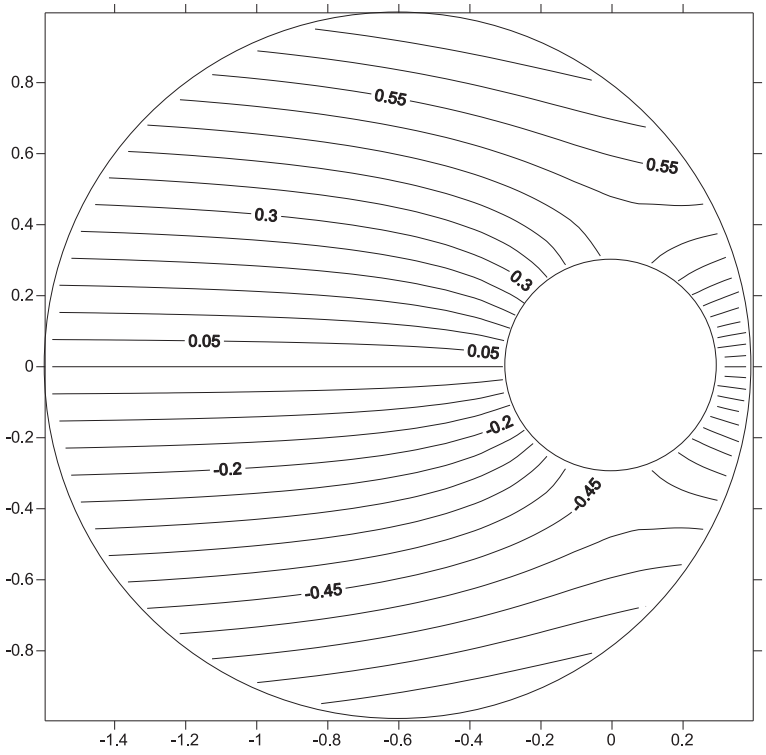

(b) Optimal solution of the original problem (N=90)

Fig. 10. The field solution of warping function in the case 1 ($\mu_1/\mu_0 = 0$).

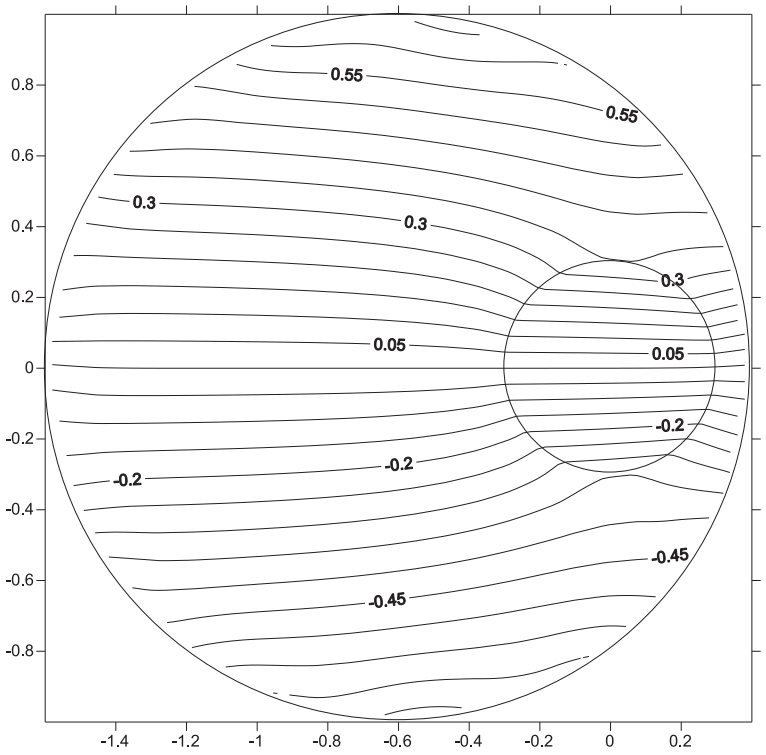

(a) Exact solution of the auxiliary problem (M=48)

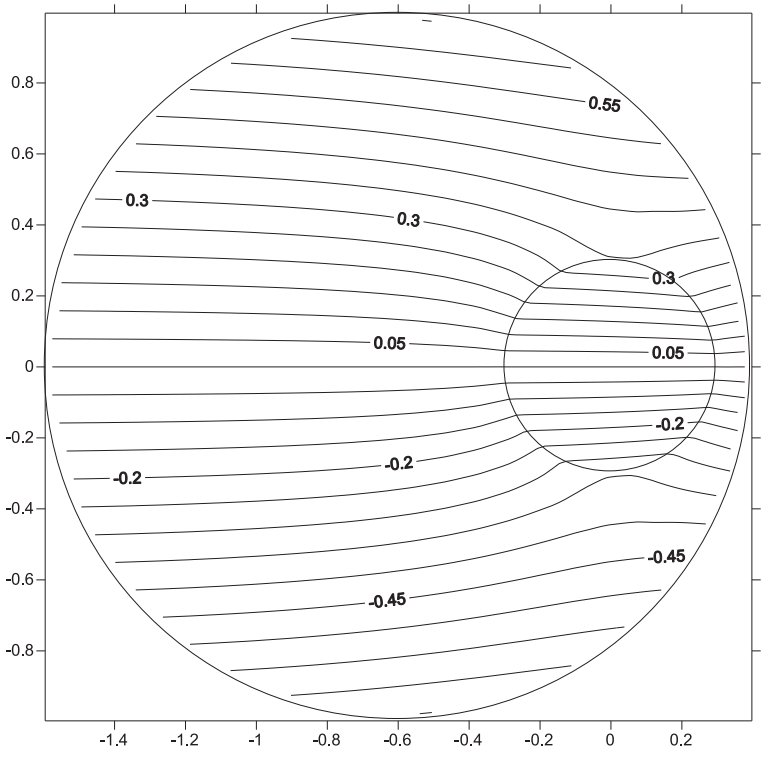

(b) Optimal solution of the original problem (N=90)

Fig. 11. The field solution of warping function in the case 1 ($\mu_1/\mu_0 = 0.2$).

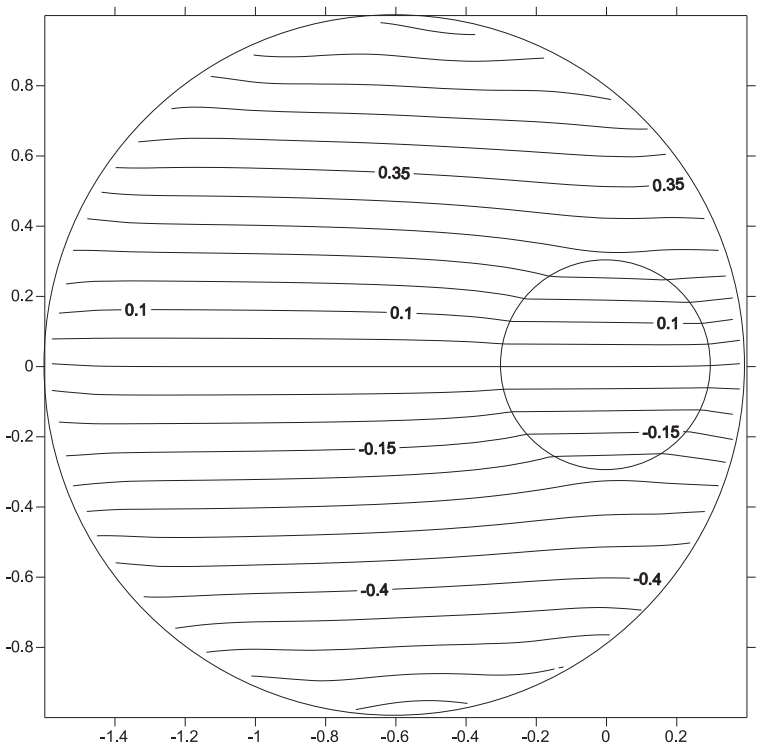

(a) Exact solution of the auxiliary problem (M=48)

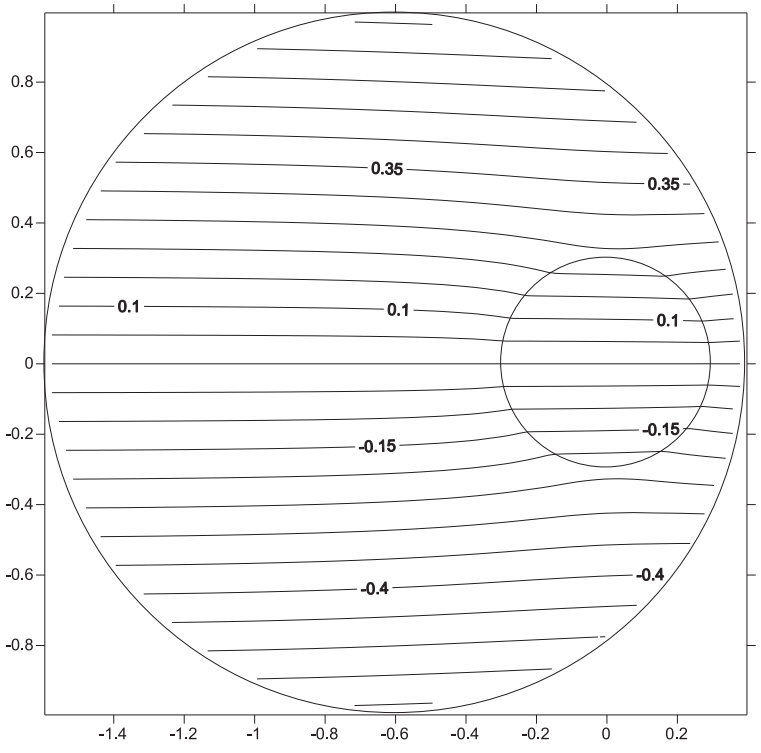

(b) Optimal solution of the original problem (N=90)

Fig. 12. The field solution of warping function in the case 1 ($\mu_1/\mu_0 = 0.6$).

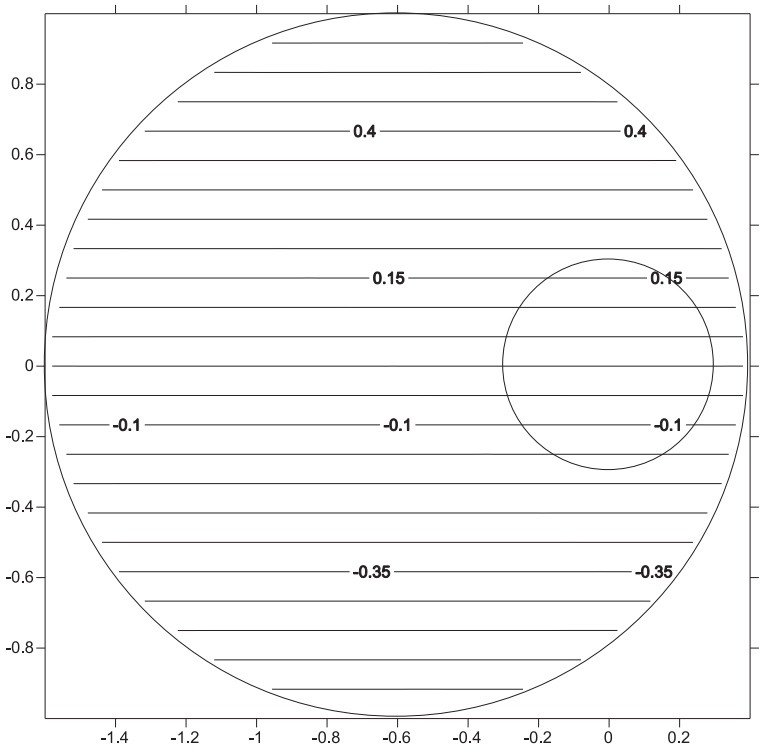

(a) Exact solution of the auxiliary problem (M=48)

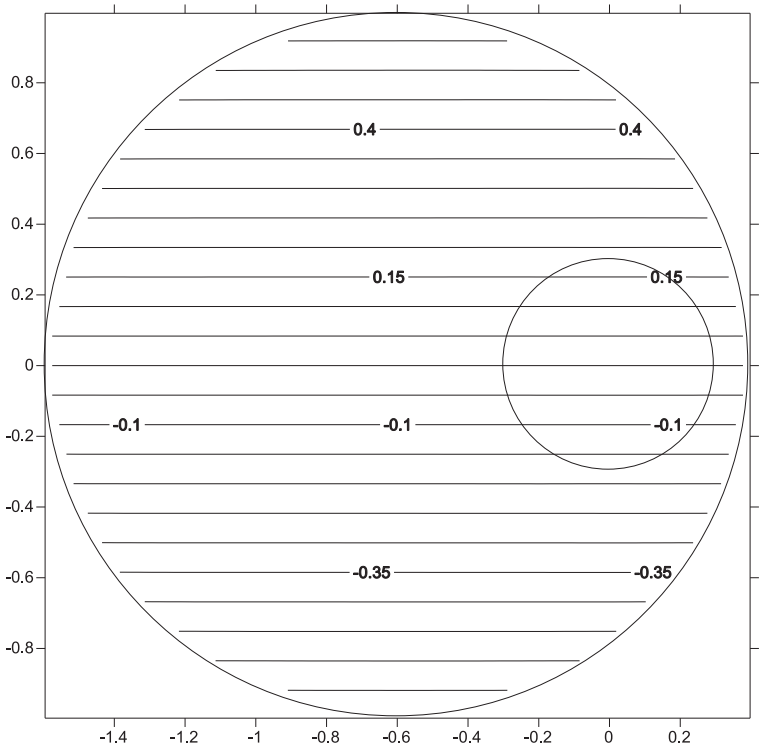

(b) Optimal solution of the original problem (N=90)

Fig. 13. The field solution of warping function in the case 1 ($\mu_1/\mu_0 = 1$).

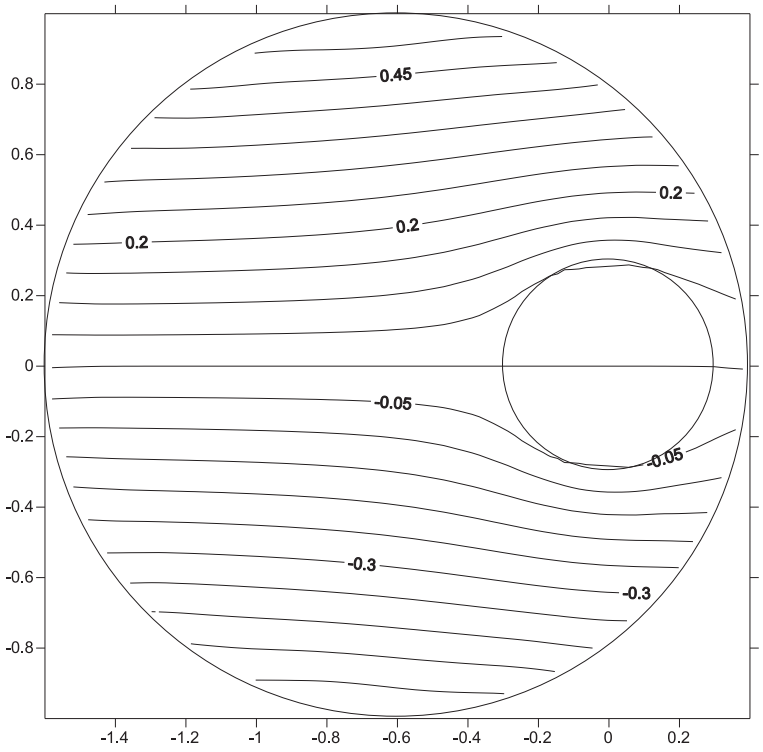

(a) Exact solution of the auxiliary problem (M=48)

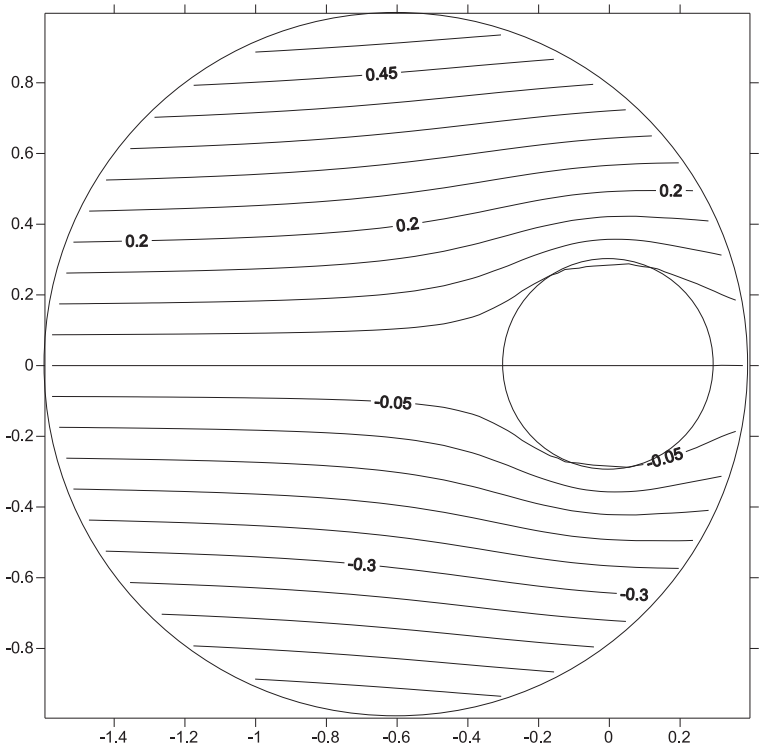

(b) Optimal solution of the original problem (N=90)

Fig. 14. The field solution of warping function in the case 1 ($\mu_1/\mu_0 = 5$).

The relationship of the real exact solution and the auxiliary solution can be written as:

$$\varphi^e(x) = \varphi^q(x) + R_M(x) \tag{39}$$

where $\varphi^e(x)$ is the exact solution of the real problem and $R_M(x) = \sum_{j=M+1}^{\infty} \upsilon_j \Omega_j(x)$. The remainder function satisfies the G.E. and it is exponential convergence as:

$$||R_M(x)|| = O\left(r^{-M}\right), r > 1 \tag{40}$$

where $r = \|x\|$. Therefore, the difference in the two solvers of space is derived as:

$$\|\varphi^e(x) - \varphi^q(x)\| = \|R_M(x)\| \le C\left(r^{-M}\right), r > 1 \tag{41}$$

where C is the bounded constant.

4.4. Error analysis in the auxiliary problem

The error norm of numerical solution of the auxiliary problem adopts the relative root mean squared (RMS) error by comparing the numerical solution with the exact solution in the auxiliary problem which is defined as shown below:

$$\text{R.M.S} = \sqrt{\frac{1}{N^F}\sum_{i=1}^{N^F}\left[\varphi^F(x_i) - \varphi^q(x_i)\right]^2} \Big/ \sqrt{\frac{1}{N^F}\sum_{i=1}^{N^F}\left[\varphi^q(x_i)\right]^2} \tag{42}$$

where N^F is the total number of field points and $\varphi^F(x_i)$ is the numerical solution of the BEM in the auxiliary problem. Besides, the error norm can also be adopted by the relative error of rigidity as follows:

$$\text{Relative error of rigidity} = \sum_{i=1}^{N^F} \frac{G^F(x_i) - G^q(x_i)}{G^q(x_i)} \tag{43}$$

Fig. 3 is shows a flowchart of the new error estimation technique. By the auxiliary problem, the error curve can be obtained through the error convergence analysis. Based on the specified criteria, the optimal number of elements can be found in the neighboring region of the corner in the error curve.

4.5. Solving the solution of the original problem

Adopting the optimal number of elements, the unknown boundary densities can be solved by collocating observation points to match the BCs in the original problem, and then the optimal solutions for the domain of interest of the original problem can be calculated.

5. Numerical examples

In this section, three cases with different cross-sections are considered. The three cases with circular, elliptical and rectangular domains given by Muskhelishvili [14], Chen and Lee [21], Katsikadelisand Sapountzakis [17] and Shams-Ahmadiand Chou [18] are solved, respectively, by using the BEM. By applying the error technique, we also derive the optimal ratio of the number of collocation elements/points between the exterior and interior boundaries.

Case 1: A circular bar with an eccentric inclusion [14,21]

In this case, a circular bar with an eccentric hole/inclusion is considered as shown in Fig. 4. The radius of the circular bar is R_0 and radius of eccentric hole/inclusion is R_1. The dimensional ratio of R_1/R_0 is 0.3 and e_x/R_0 is 0.6. The shear modulus ratio μ_1/μ_0 is considered 0, 0.2, 0.6, 1, and 5 in numerical results. Figs. 5–9 are shown the result of the relative error of rigidity and R.M.S error, respectively. After comparing with the literature [14,21], we can obtain good results using more than 60 elements. So, the optimal number of elements will choose about 90 elements in this case. After adopting optimal number of elements to solve the original problem by using the BEM formulation, we can obtain the field solutions of the warping function and the shear flow as shown in Figs. 10–19, respectively.

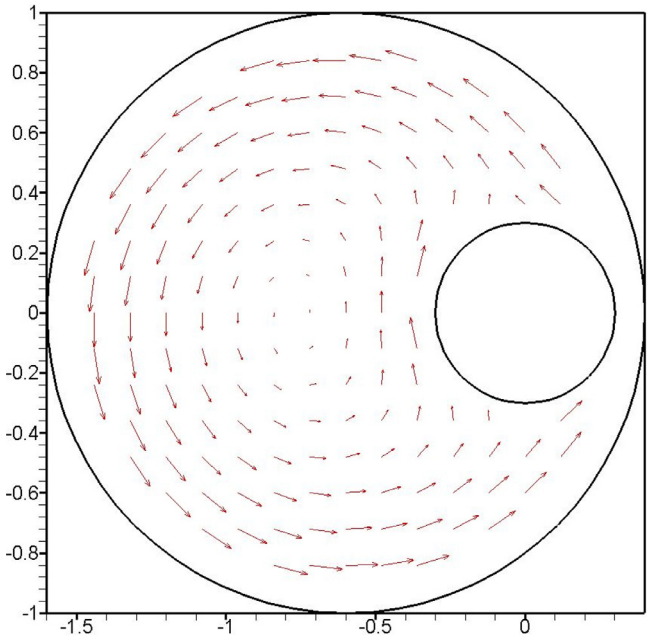

Fig. 15. The field solution of shear flow by adopting the optimal number of elements in the case 1 ($\mu_1/\mu_0 = 0$).

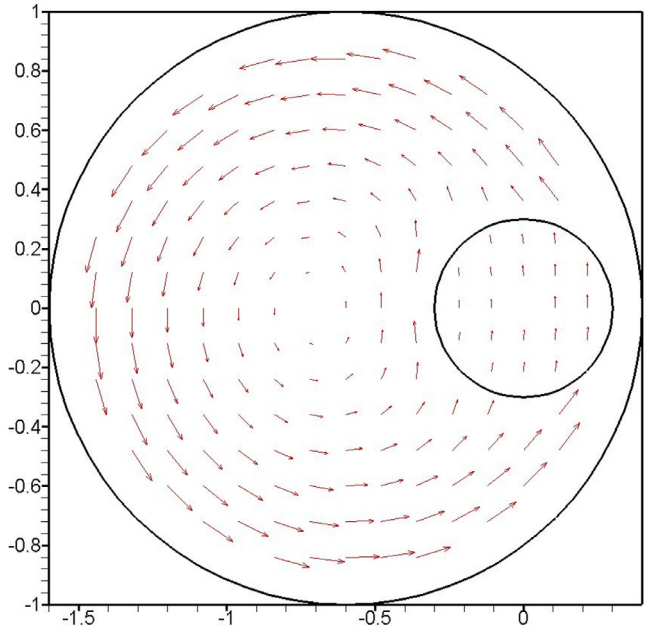

Fig. 16. The field solution of shear flow by adopting the optimal number of elements in the case 1 ($\mu_1/\mu_0 = 0.2$).

Through the error technique, the optimal results of torsional rigidity compared with Muskhelishvili's solution [14] for different shear modulus ratio μ_1/μ_0 are listed in Table 2. Muskhelishvili's solution [14] is given below:

$$G = \mu_0 I + (\mu_1 - \mu_0) I' - \frac{\pi R_1^2 e_x^2 (\mu_1 - \mu_0)^2}{(\mu_1 + \mu_0)} - 2\mu_0 \pi e_x^2 \nu \rho_1^2 \sum_{k=1}^{\infty} \frac{\alpha^k \nu^k}{(1 - a^2 \rho_1^2 \alpha^k)}, \tag{44}$$

where

$$I = \pi R_0^4/2, \tag{45}$$

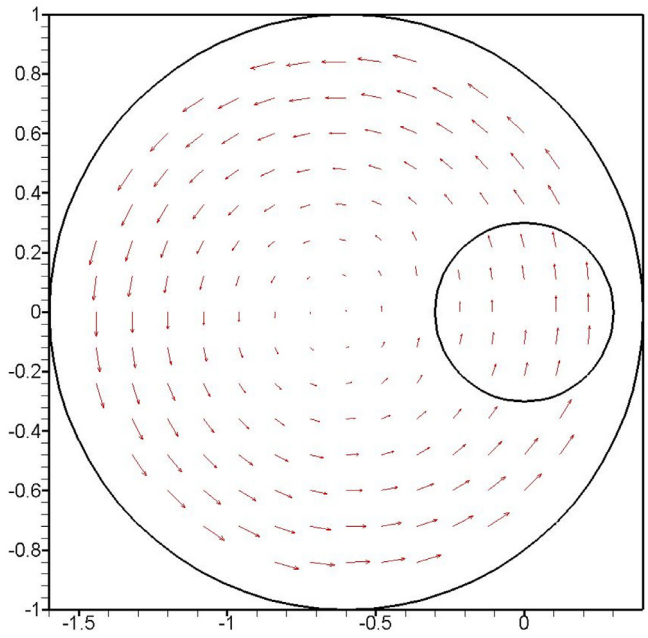

Fig. 17. The field solution of shear flow by adopting the optimal number of elements in the case 1 ($\mu_1/\mu_0 = 0.6$).

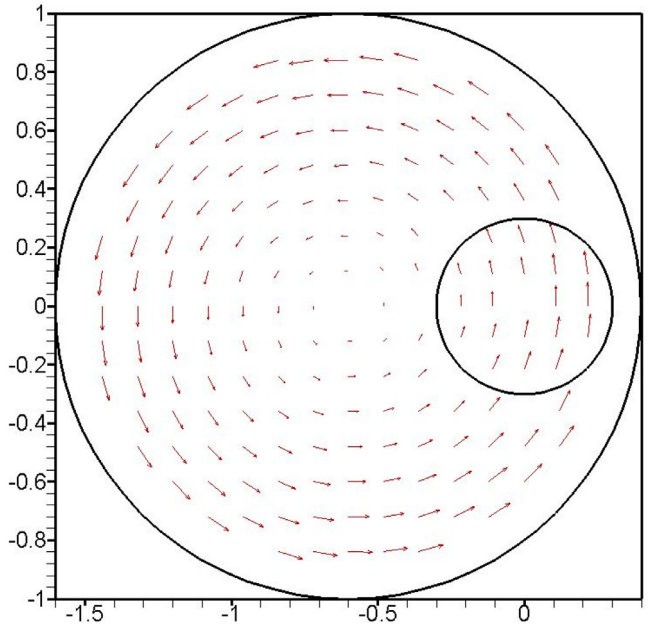

Fig. 18. The field solution of shear flow by adopting the optimal number of elements in the case 1 ($\mu_1/\mu_0 = 1$).

Table 2
Comparison with torsional rigidity in the case 1.

$2\,G/\pi\mu_0 R_0{}^4$			
μ_1/μ_0	Muskhelishvili (1953)	Chen and Lee (2009)	BEM
0.0	0.82370	0.82370	0.82357
0.2	0.89180	0.89180	0.89165
0.6	0.96246	0.96246	0.96230
1.0	1.00000	1.00000	0.99984
5.0	1.10800	1.10800	1.10783

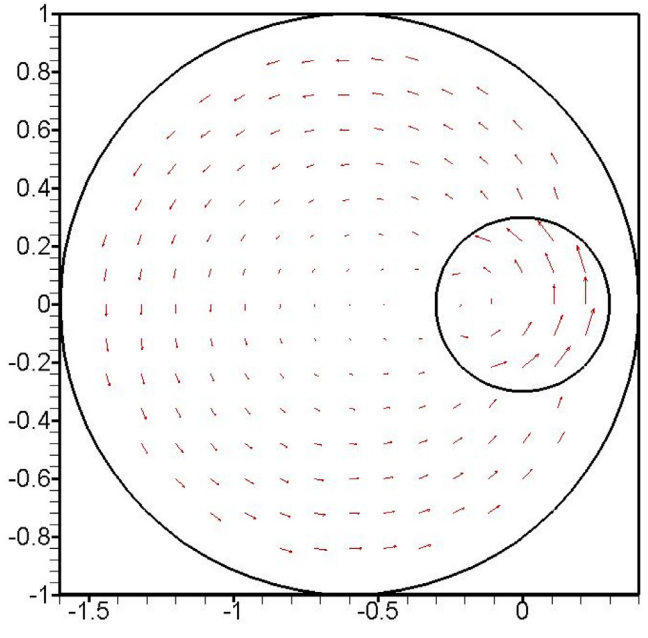

Fig. 19. The field solution of shear flow by adopting the optimal number of elements in the case 1 ($\mu_1/\mu_0 = 5$).

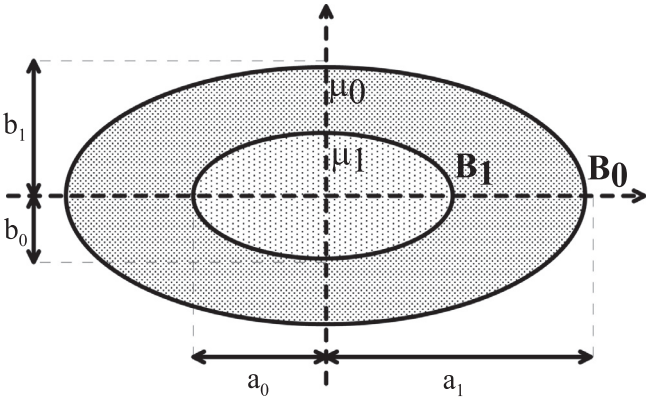

Fig. 20. Sketch of problem in the case 2.

$$I' = \pi R_1^4/2 + \pi R_1^2 e_x^2, \tag{46}$$

$$a = e_x/\sqrt{\left(R_1^2 - R_0^2\right)^2 - 2e_x^2\left(R_1^2 + R_0^2\right) + e_x^4}, \tag{47}$$

$$\alpha = \rho_1^2/\rho_0^2, \tag{48}$$

$$\nu = \left(\mu_0 - \mu_1\right)/\left(\mu_0 + \mu_1\right), \tag{49}$$

$$\rho_1 = \sqrt{1 + 4R_1^2 a^2} - 1/2R_1 a^2, \tag{50}$$

$$\rho_1 = \sqrt{1 + 4R_1^2 a^2} - 1/2R_1 a^2. \tag{51}$$

By comparing with the Table 2, the presented results matched well with the Muskhelishvili solution [14].The relative error of rigidity is presented in Tables 5–9. N_0/N_1 denotes the ratio of element number in boundary. We can see that the error of results is different when adopting corresponding configurations of the distribution of the number of elements on the different boundaries, thus we can obtain better results

Table 3
Comparison of the torsional rigidity in the case 2.

$G/\mu_0 a_1{}^4$		
μ_1/μ_0	Katsikadelis (1985)	BEM
0.0	0.2953	0.2944
0.2	0.2992	0.2984
0.4	0.3032	0.3023
0.6	0.3071	0.3062
0.8	0.3111	0.3101
1.0	0.3150	0.3141

Table 4
Comparison of the torsional rigidity in the case 3.

$G/\mu_0 L^4$		
μ_1/μ_0	Shams-Ahmadi and Chou (1997)	BEM
0.0	0.1345	0.1343
1.0	0.1405	0.1405
2.0	0.1465	0.1467
3.0	0.1524	0.1528
5.0	0.1644	0.1651

than the average distribution of the number elements on the different boundary.

Case 2: An elliptic bar with an elliptic inclusion [17]

Here, we consider a composite cross-section consisting of two concentric, geometrically similar ellipses with a_1/a_0=0.5, b_0/a_0=0.5 and b_1/b_0=0.25, as shown in Fig. 20. The ratio of shear modulus μ_1/μ_0 is using 0, 0.2, 0.4, 0.6, 0.8, and 1 in this case. The results of the relative error of rigidity and R.M.S error by using the BEM are shown in Figs. 21–26, respectively. The results of the literature **[**17**]** are shown simultaneously in Figs. 21–26. Comparing Figs. 21–26, we can find good results, when Trefftz term and the number of boundary elements are more than the 24 and 90, respectively. In this case, we choose about 90 elements to solve the original problem. We can obtain the field solutions of the warping function and the shear flow for different ratio of shear module by using the BEM as shown in Figs. 27–38, respectively. The field solution of the warping function for different μ_1/μ_0 are shown in Figs. 29–32. We can find that results are agreeable. Figs. 33–38 show the distribution of shear flow by adopting the optimal number of elements for different μ_1/μ_0.

The optimal results of torsional rigidity compared with Katsikadelis's solution [17] for different values of $\mu_1/\mu_0$are listed in Table 3. Tables 10–15 for μ_1/μ_0=0, 0.2, 0.4, 0.6, 0.8, 1.0 show the relative error of rigidity. The preferred average distribution of the number of elements can be obtained by comparing Tables 10–15.

Case 3: A rectangular bar with a circular inclusion [18]

Here, we consider a rectangular bar of length L with a circular inclusion of radius $L/4$, as shown in Fig. 39. The results of the relative error of rigidity and R.M.S error for the ratio of shear module μ_1/μ_0 = 0, 1, 2, 3, and 5 are shown in Figs. 40–44, respectively. The dotted line is the result of the literature [18] in Figs. 40(a)–44(a). We can obtain the optimal number of elements of 96 by comparing Figs. 40–44 in this case. By using the optimal number of elements and BEM formulation to solve the original problem, we can obtain the field solutions of the warping function and the shear flow for μ_1/μ_0=0, 1, 2, 3, and 5 in Figs. 45–54, respectively.

The optimal results of torsional rigidity compared with Shams-Ahmadi's solution [18] for different ratio of shear module μ_1/μ_0 are listed in Table 4.The relative error of rigidity in different ratio of element number for μ_1/μ_0=0, 1, 2, 3, 5 are shown in Tables 15–19. We can obtain better results than the average distribution of the number elements on the different boundary.

Table 5
Relative error of rigidity for different N_0/N_1 in a circular case with an eccentric inclusion (μ_1/μ_0 = 0).

N_0/N_1	Relative error of rigidity
1/9	0.11660
1/8	0.08347
1/5	0.10547
1/4	0.04333
1/2	0.01106
1/1	0.00607
2/1	0.00724
4/1	0.01632
5/1	0.02315
8/1	0.05385
9/1	0.06922

Table 6
Relative error of rigidity for different N_0/N_1 in a circular case with an eccentric inclusion (μ_1/μ_0 = 0.2).

N_0/N_1	Relative error of rigidity
1/9	0.14387
1/8	0.11372
1/5	0.07804
1/4	0.04304
1/2	0.01387
1/1	0.00651
2/1	0.00487
4/1	0.00701
5/1	0.00908
8/1	0.01854
9/1	0.02324

Table 7
Relative error of rigidity for different N_0/N_1 in a circular case with an eccentric inclusion (μ_1/μ_0 = 0.6).

N_0/N_1	Relative error of rigidity
1/9	0.15825
1/8	0.12987
1/5	0.06673
1/4	0.04328
1/2	0.01498
1/1	0.00657
2/1	0.00365
4/1	0.00255
5/1	0.00243
8/1	0.00245
9/1	0.00268

Table 8
Relative error of rigidity for different N_0/N_1 in a circular case with an eccentric inclusion (μ_1/μ_0 = 1).

N_0/N_1	Relative error of rigidity
1/9	0.16104
1/8	0.13216
1/5	0.06065
1/4	0.04244
1/2	0.01540
1/1	0.00679
2/1	0.00361
4/1	0.00198
5/1	0.00152
8/1	0.00015
9/1	0.00029

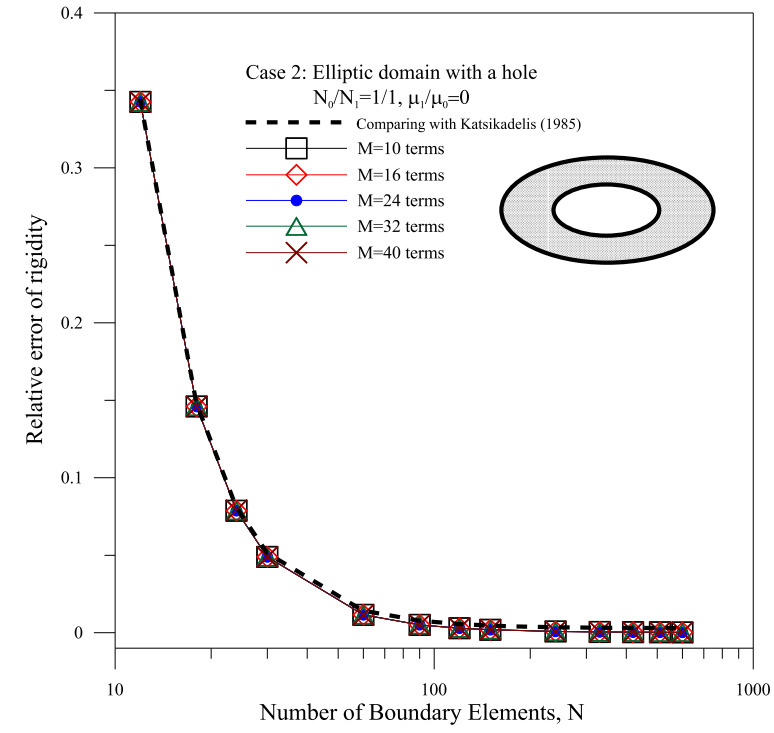

(a) Relative error of rigidity

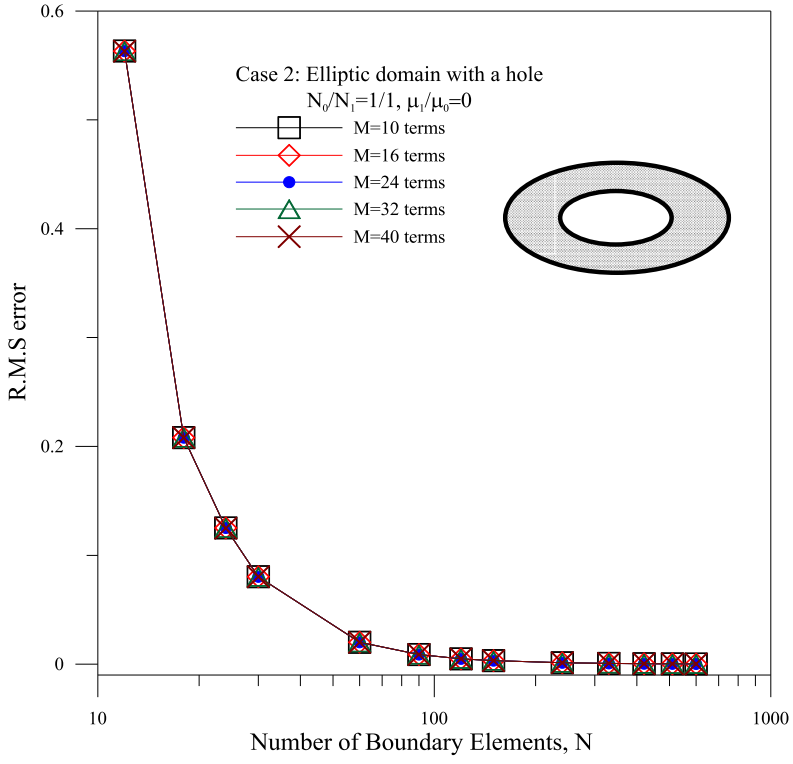

(b) R.M.S error

Fig. 21. The error analysis versus the number of boundary elements for the different terms of Trefftz basis in the case 2 ($\mu_1/\mu_0 = 0$).

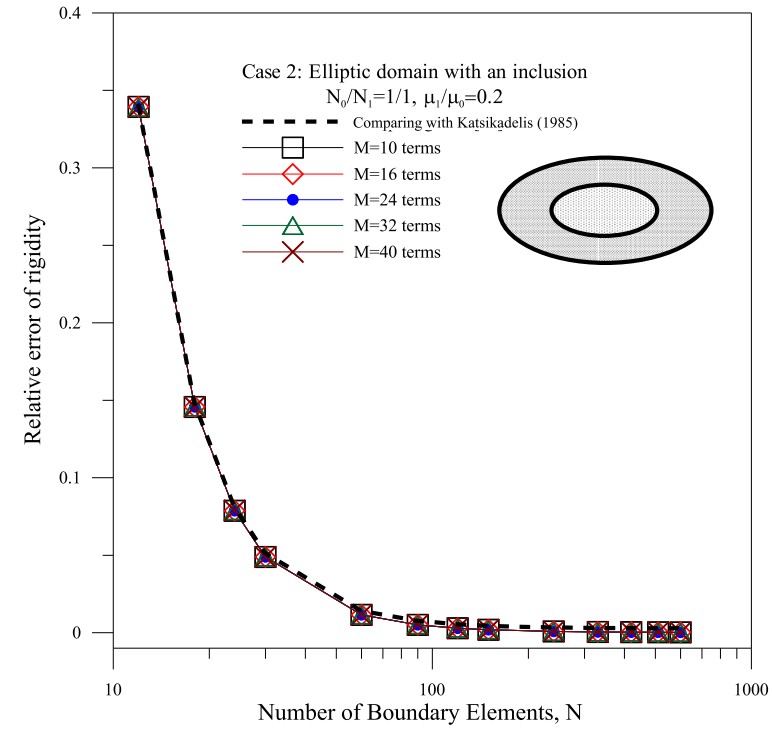

(a) Relative error of rigidity

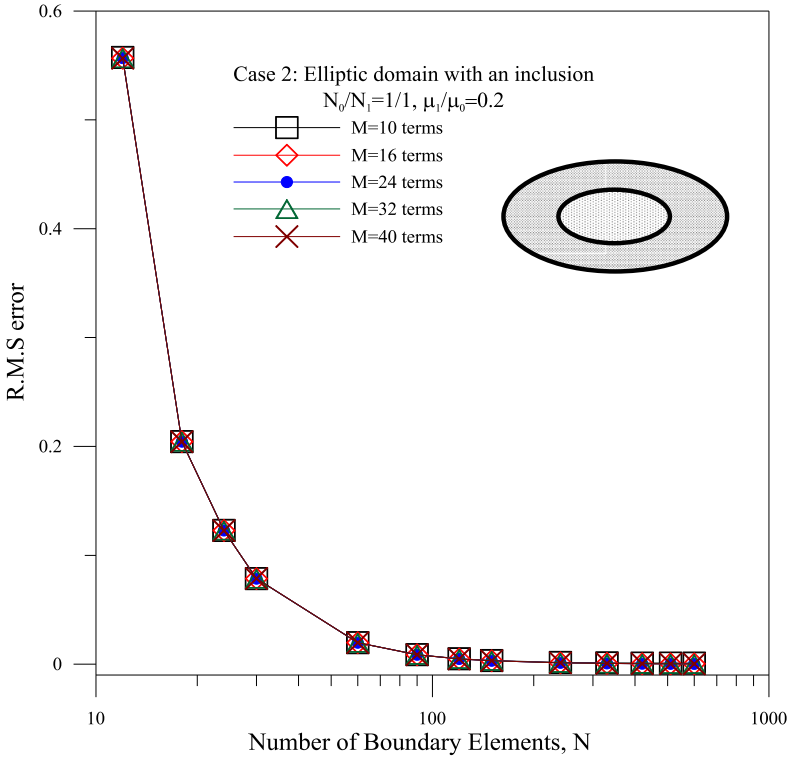

(b) R.M.S error

Fig. 22. The error analysis versus the number of boundary elements for the different terms of Trefftz basis in the case 2 ($\mu_1/\mu_0 = 0.2$).

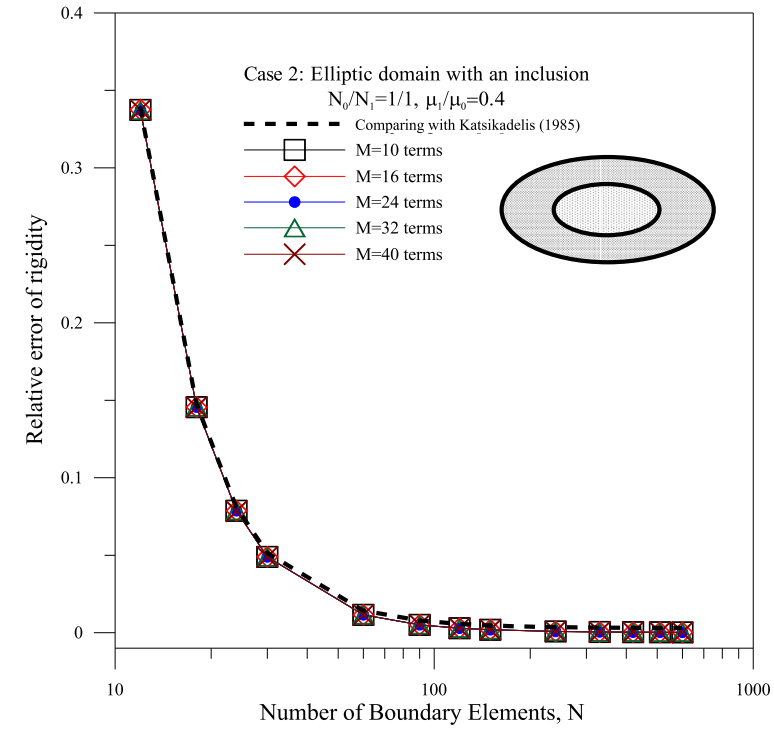

(a) Relative error of rigidity

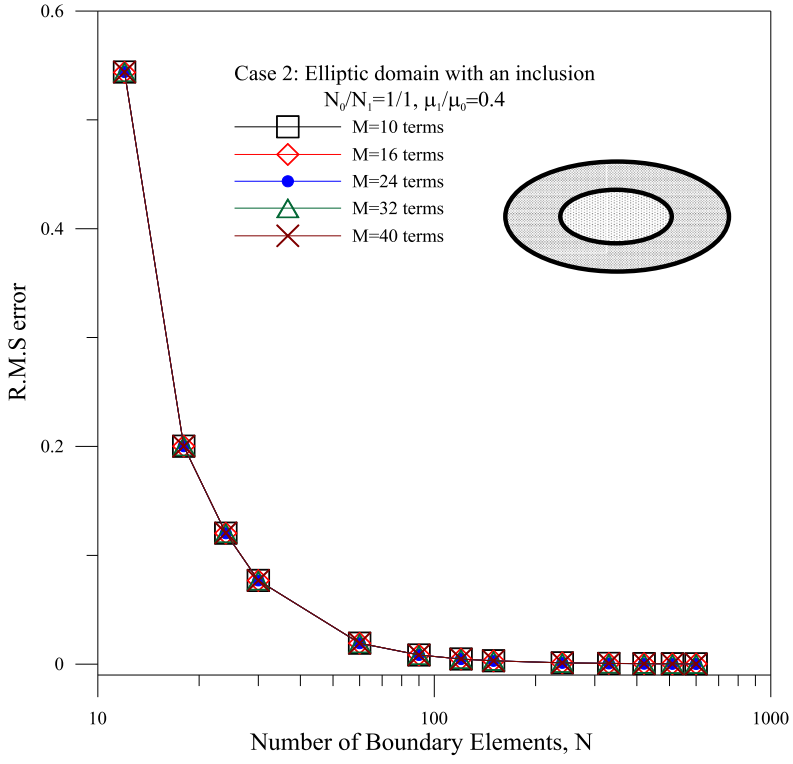

(b) R.M.S error

Fig. 23. The error analysis versus the number of boundary elements for the different terms of Trefftz basis in the case 2 ($\mu_1/\mu_0 = 0.4$).

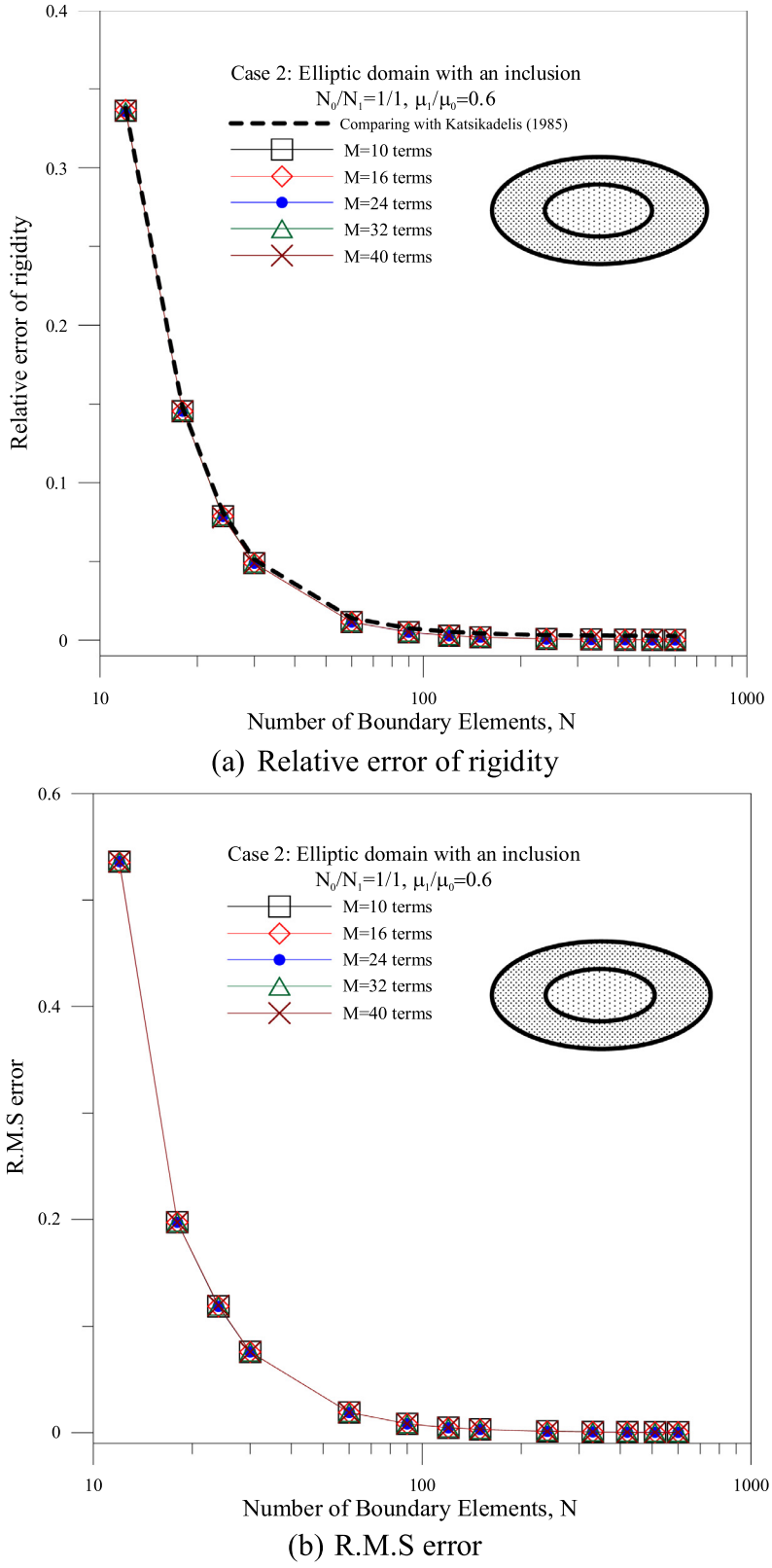

Fig. 24. The error analysis versus the number of boundary elements for the different terms of Trefftz basis in the case 2 ($\mu_1/\mu_0 = 0.6$).

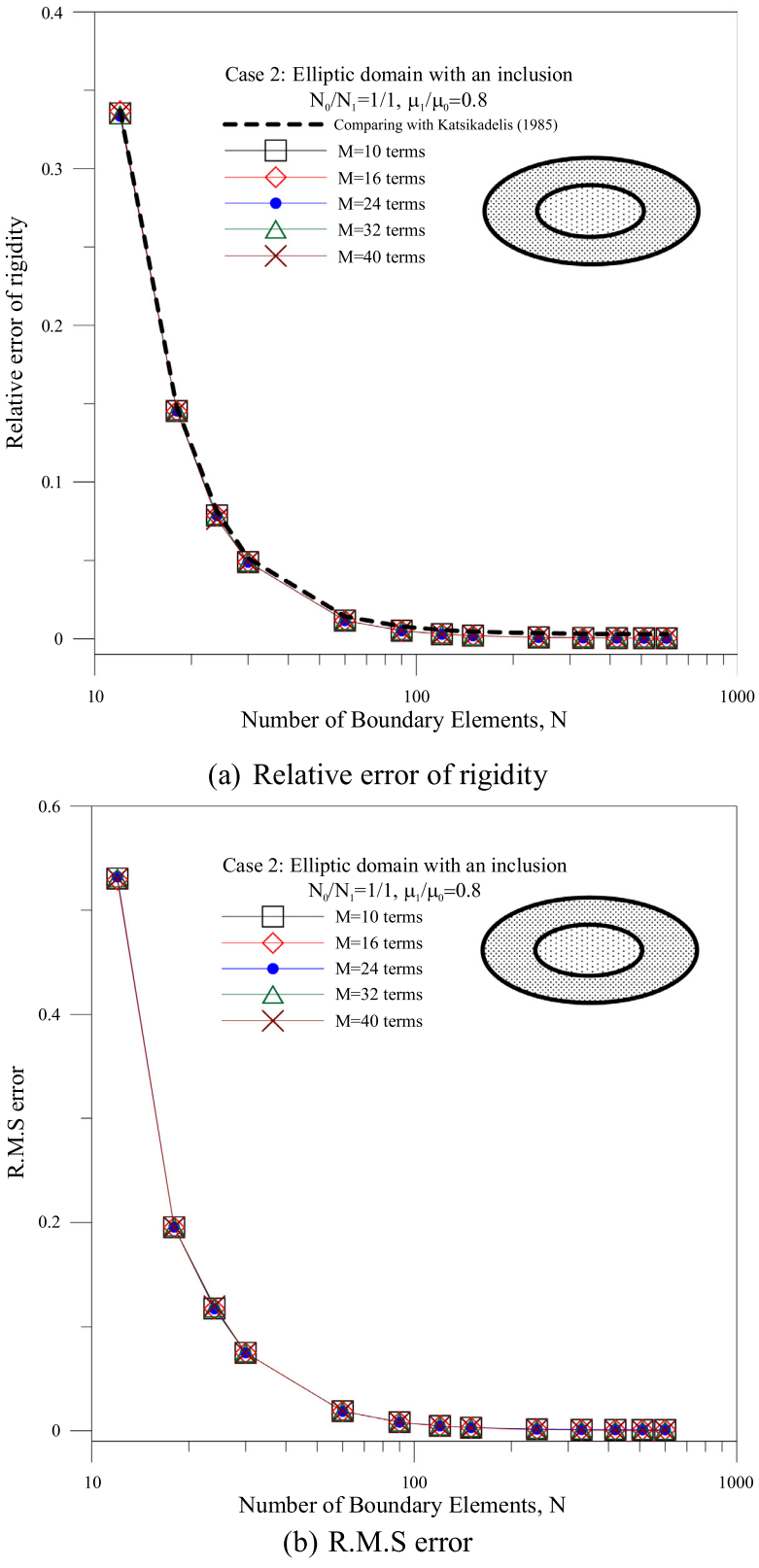

Fig. 25. The error analysis versus the number of boundary elements for the different terms of Trefftz basis in the case 2 ($\mu_1/\mu_0 = 0.8$).

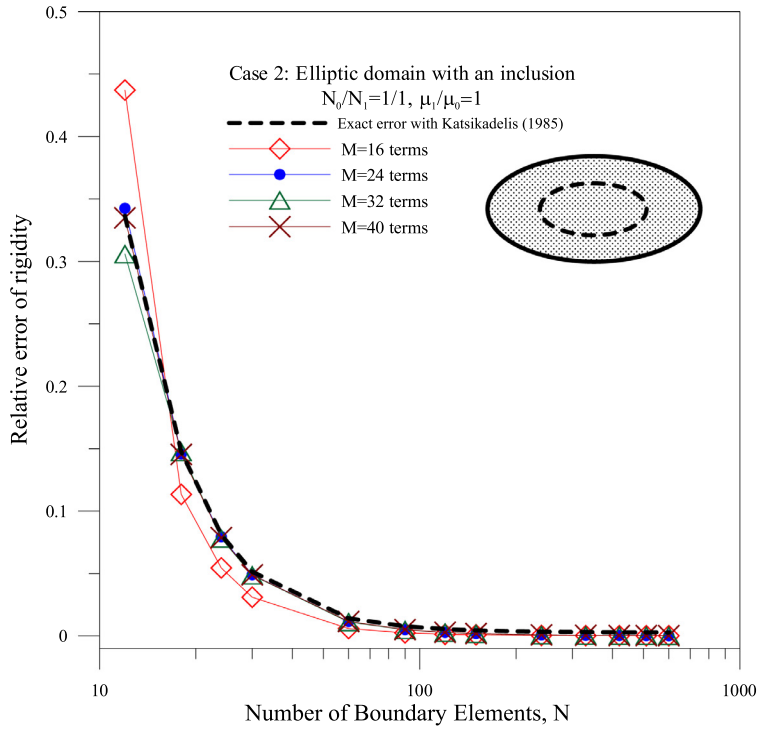

(a) Relative error of rigidity

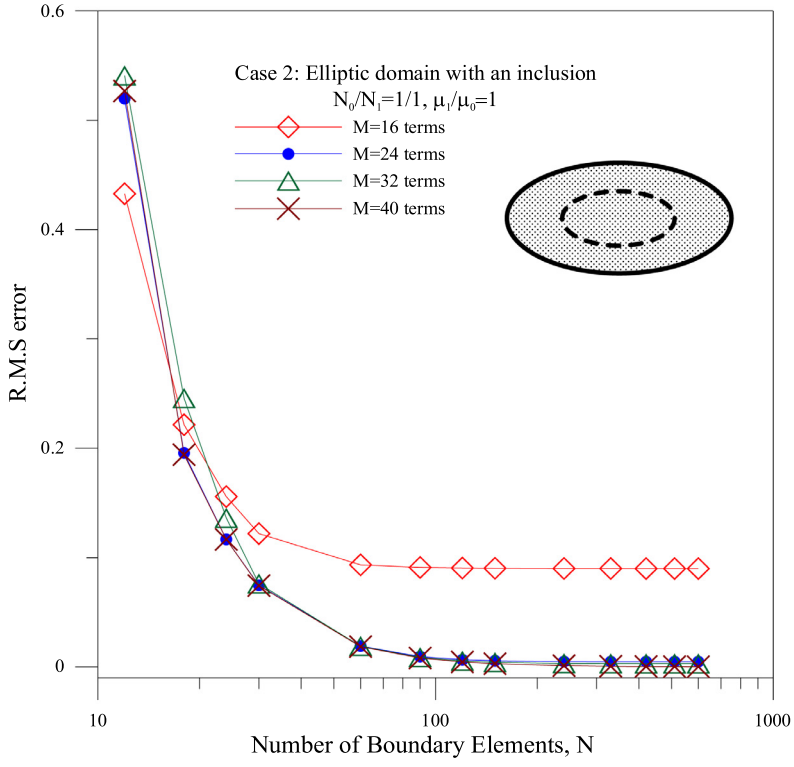

(b) R.M.S error

Fig. 26. The error analysis versus the number of boundary elements for the different terms of Trefftz basis in the case 2 ($\mu_1/\mu_0 = 1$).

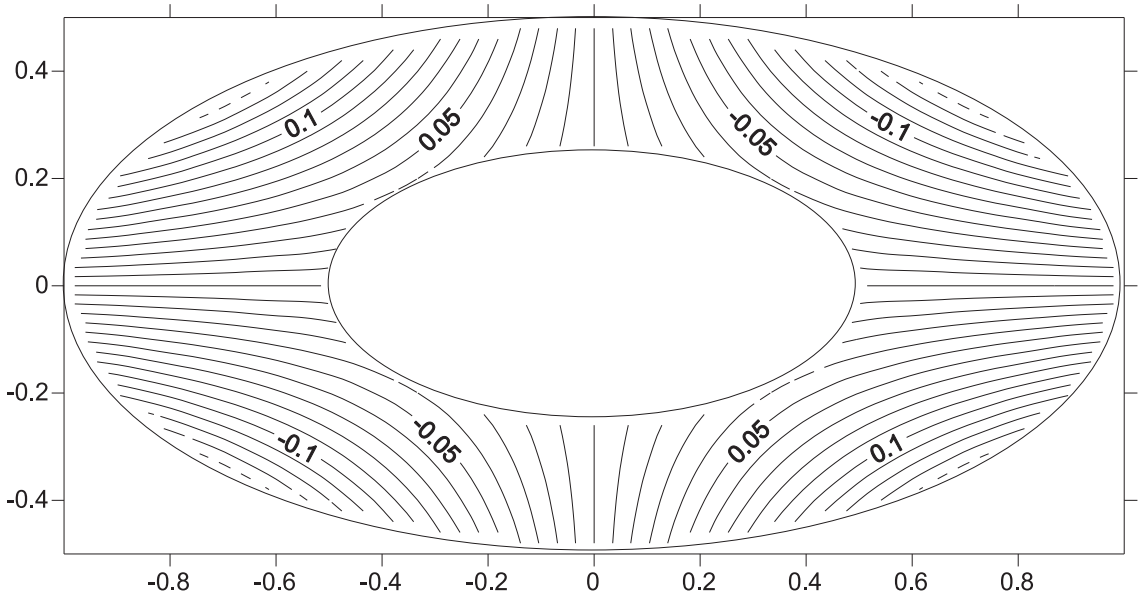

(a) Exact solution of the auxiliary problem (M=40)

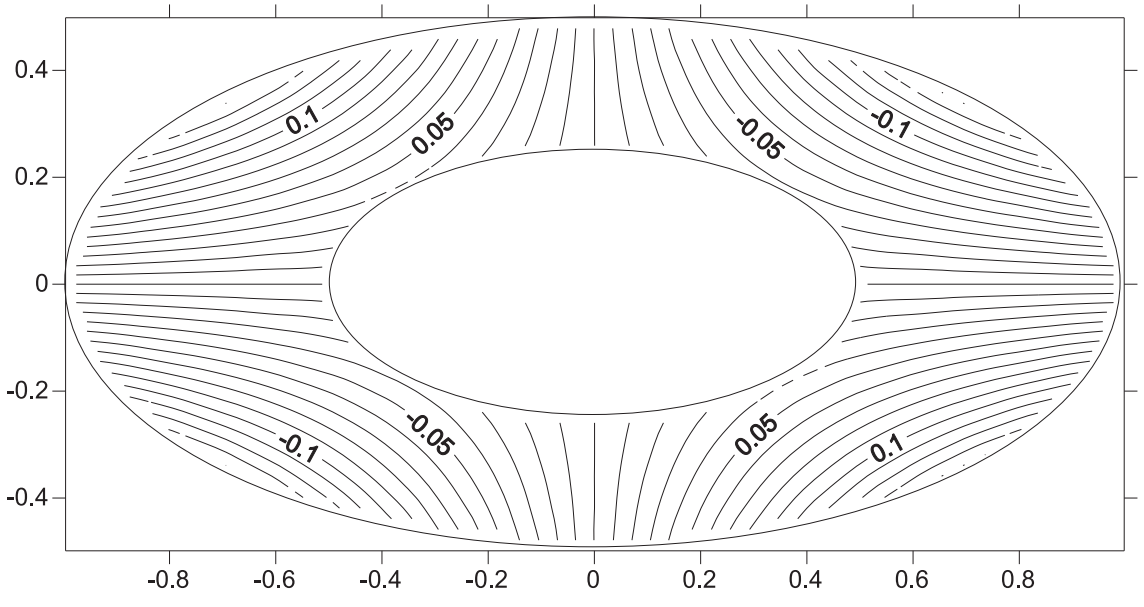

(b) Optimal solution of the original problem (N=90)

Fig. 27. The field solution of warping function in the case 2 ($\mu_1/\mu_0 = 0$).

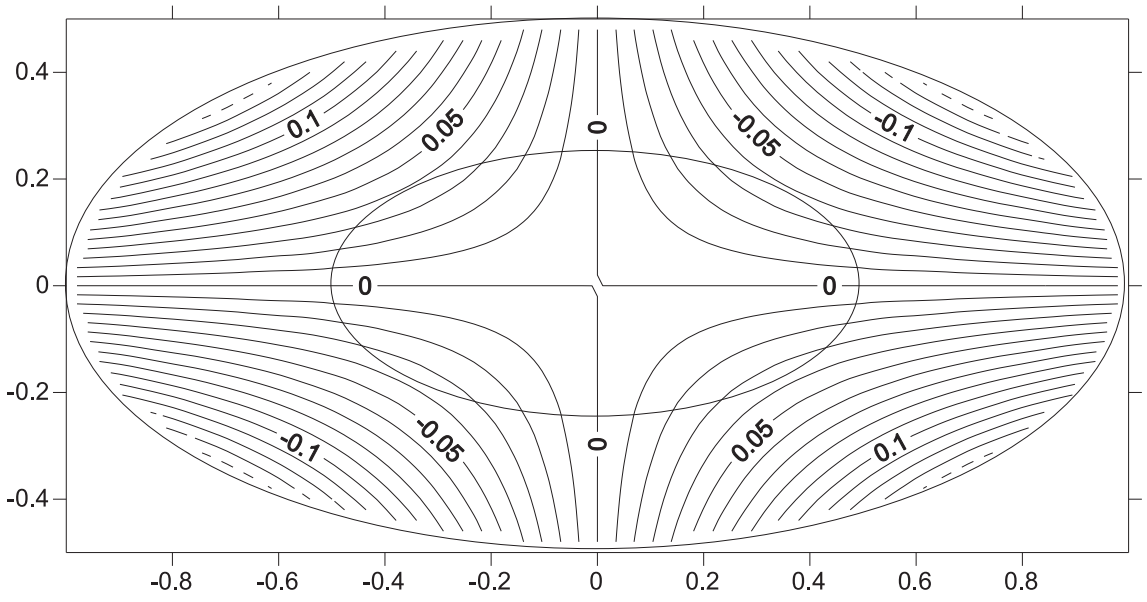

(a) Exact solution of the auxiliary problem (M=40)

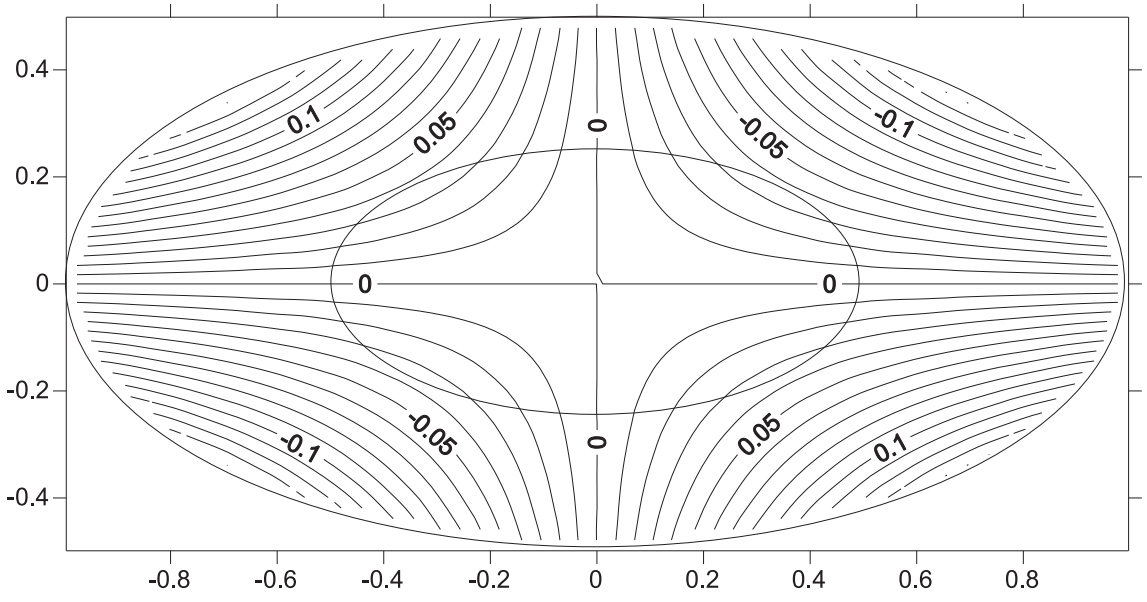

(b) Optimal solution of the original problem (N=90)

Fig. 28. The field solution of warping function in the case 2 ($\mu_1/\mu_0 = 0.2$).

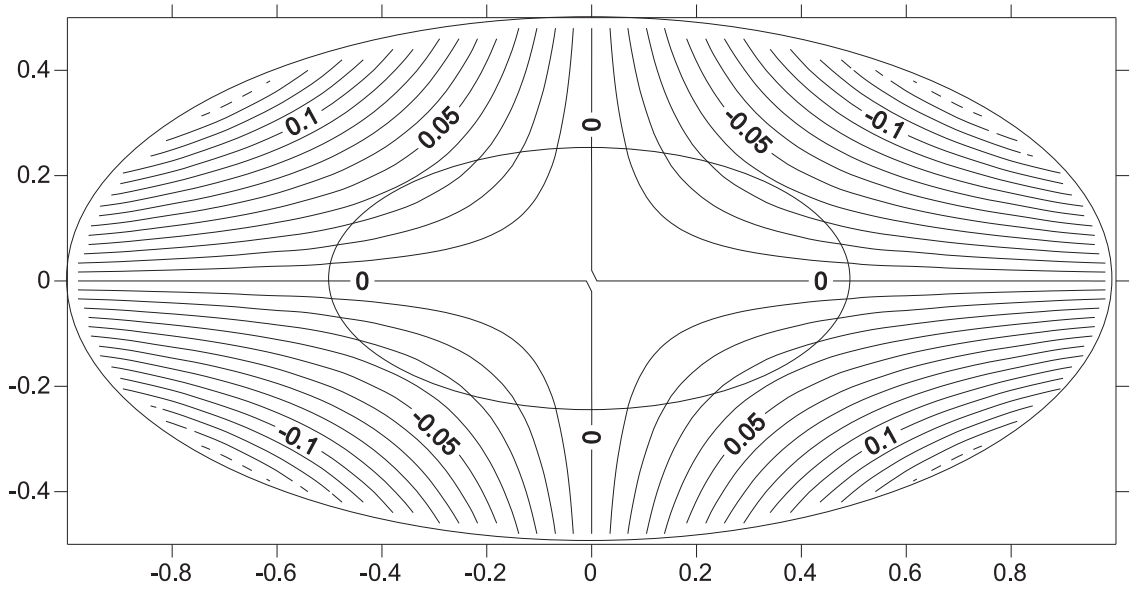

(a) Exact solution of the auxiliary problem (M=40)

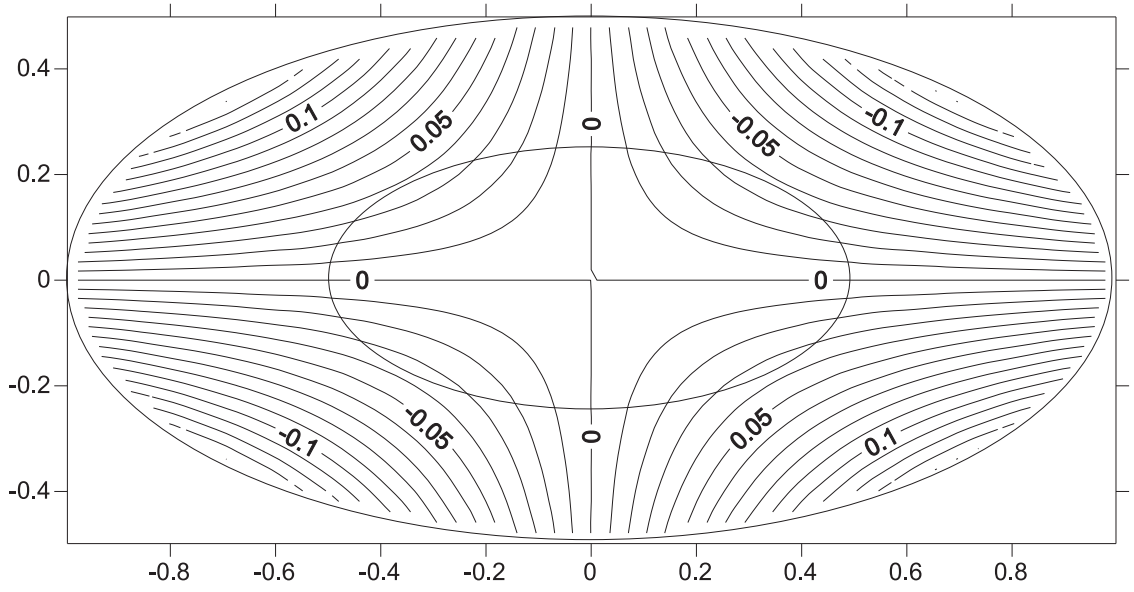

(b) Optimal solution of the original problem (N=90)

Fig. 29. The field solution of warping function in the case 2 ($\mu_1/\mu_0 = 0.4$).

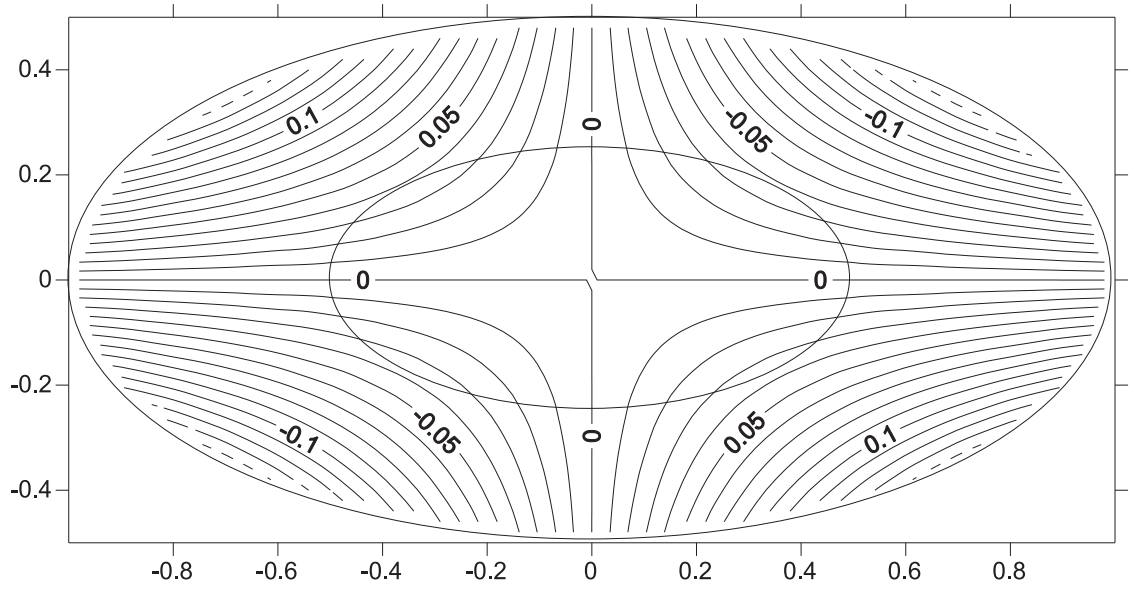

(a) Exact solution of the auxiliary problem (M=40)

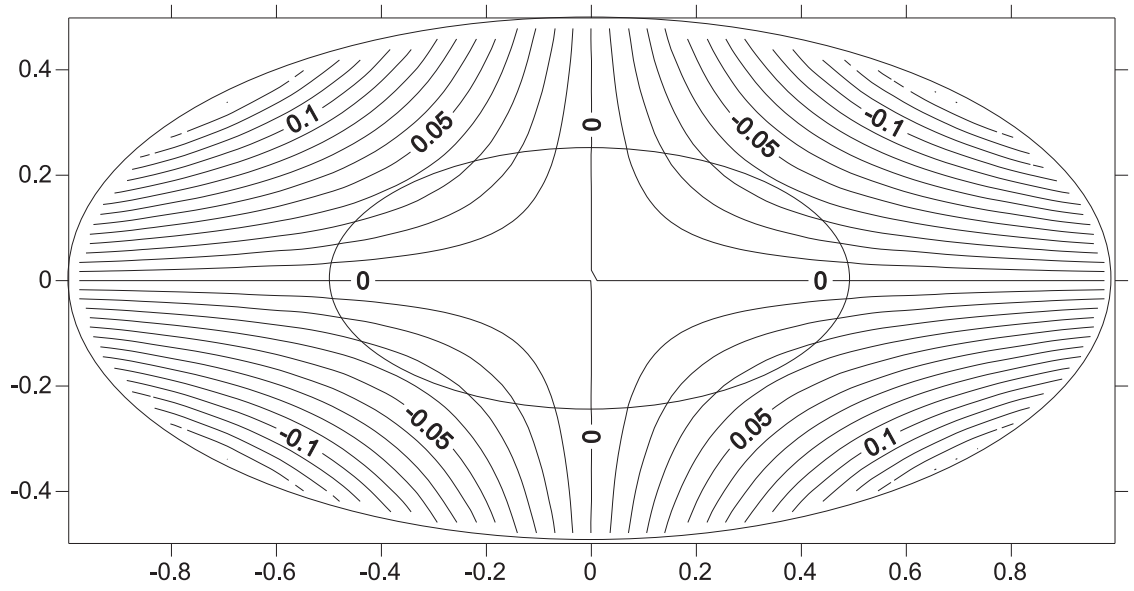

(b) Optimal solution of the original problem (N=90)

Fig. 30. The field solution of warping function in the case 2 ($\mu_1/\mu_0 = 0.6$).

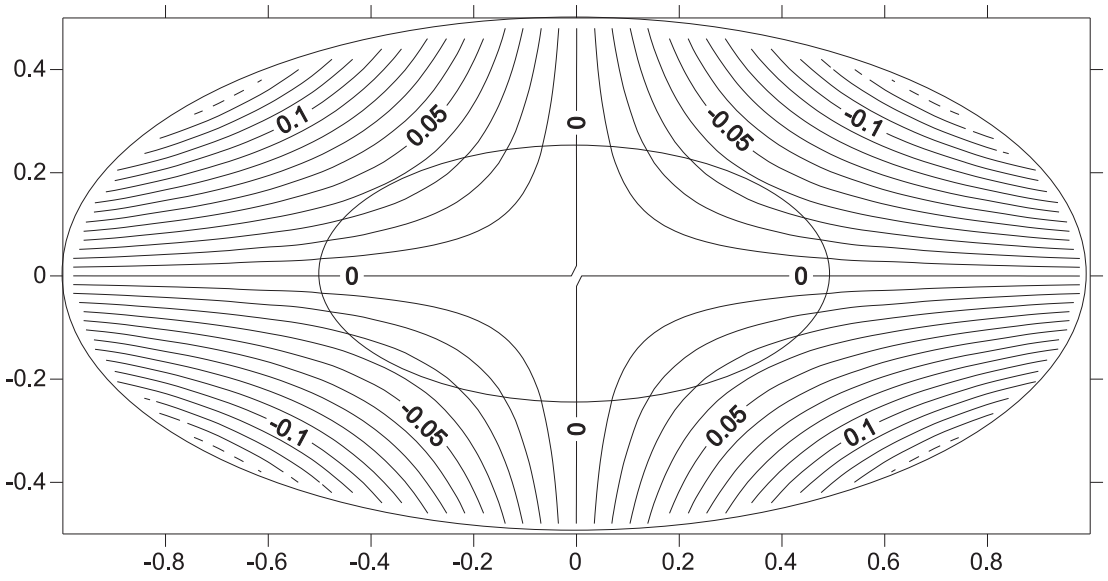

(a) Exact solution of the auxiliary problem (M=40)

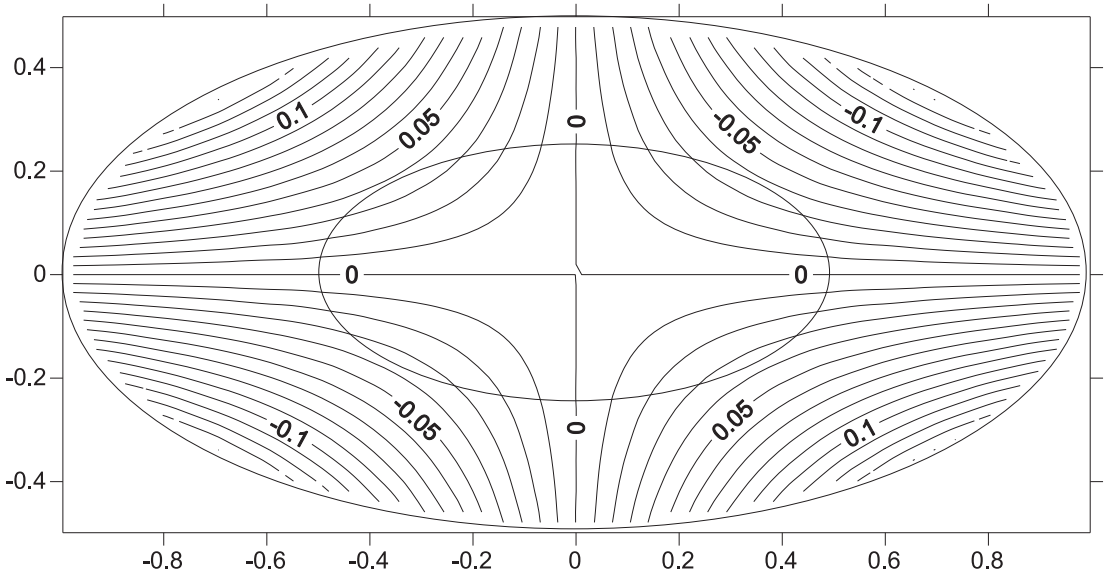

(b) Optimal solution of the original problem (N=90)

Fig. 31. The field solution of warping function in the case 2 ($\mu_1/\mu_0 = 0.8$).

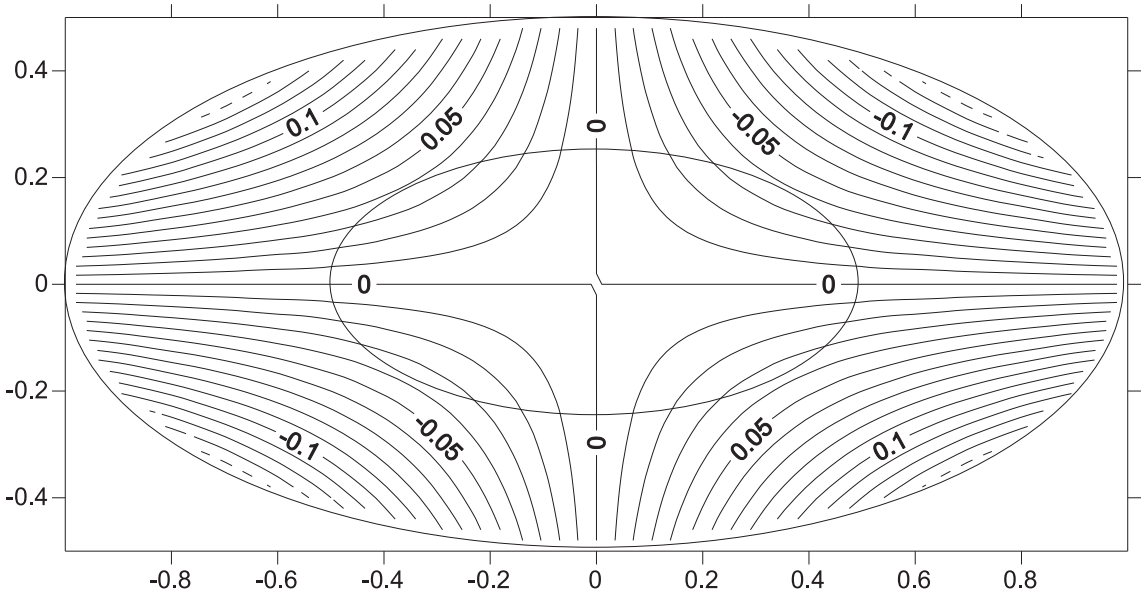

(a) Exact solution of the auxiliary problem (M=40)

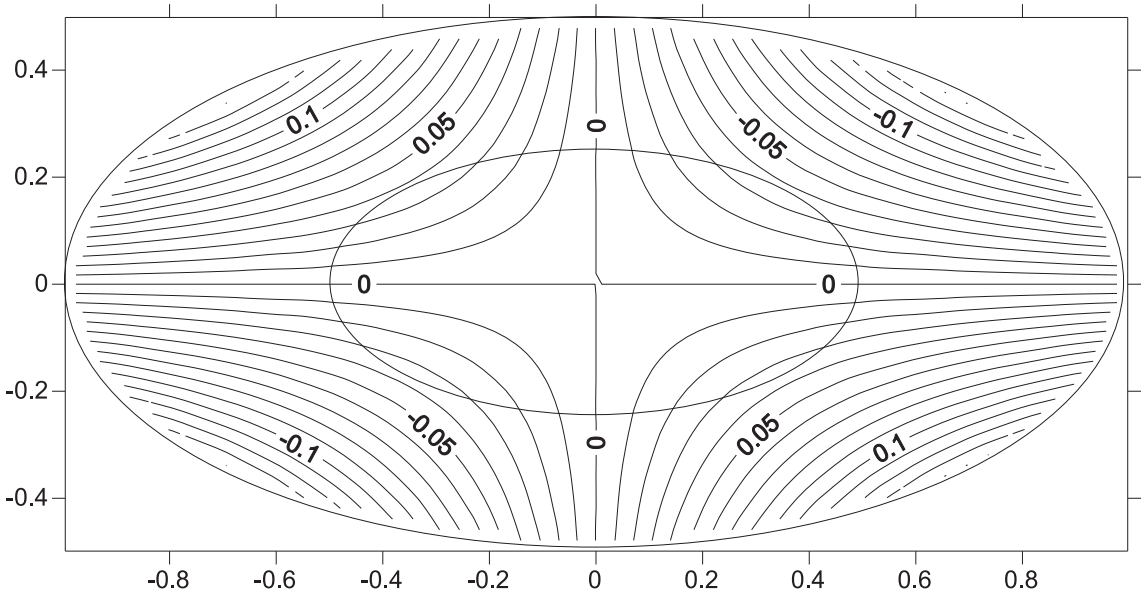

(b) Optimal solution of the original problem (N=90)

Fig. 32. The field solution of warping function in the case 2 ($\mu_1/\mu_0 = 1$).

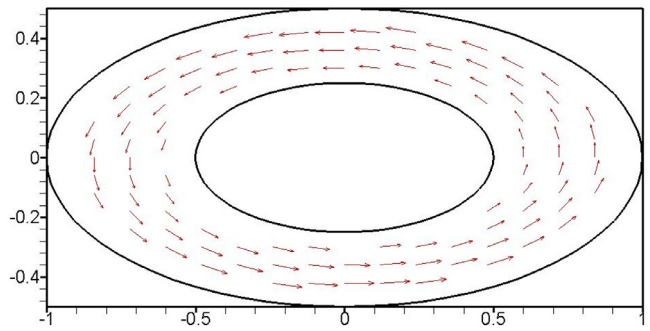

Fig. 33. The field solution of shear flow by adopting the optimal number of elements in the case 2 ($\mu_1/\mu_0 = 0$).

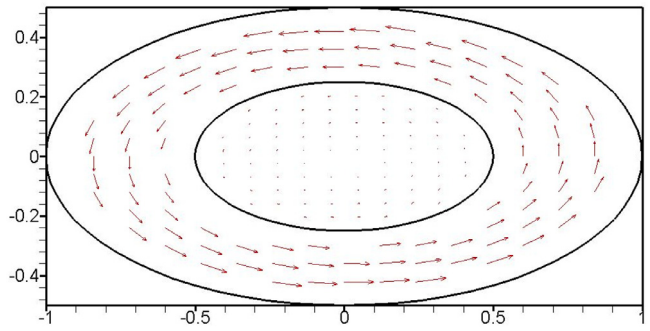

Fig. 34. The field solution of shear flow by adopting the optimal number of elements in the case 2 ($\mu_1/\mu_0 = 0.2$).

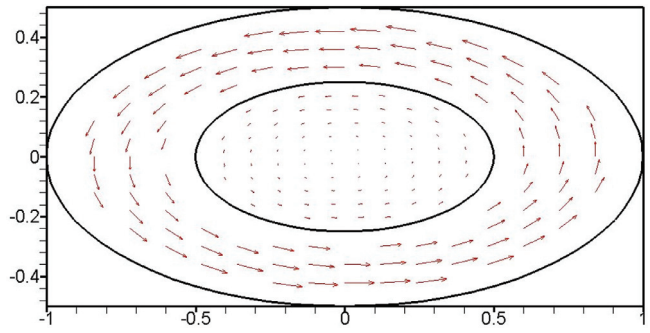

Fig. 35. The field solution of shear flow by adopting the optimal number of elements in the case 2 ($\mu_1/\mu_0 = 0.4$).

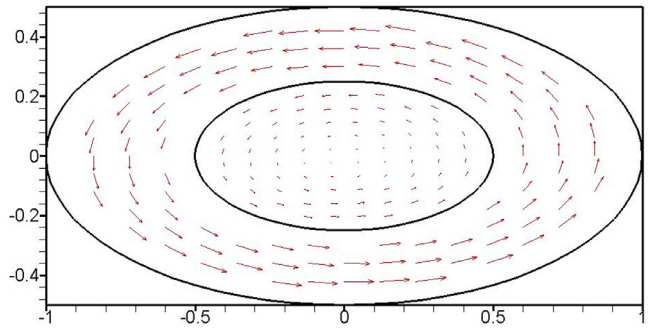

Fig. 36. The field solution of shear flow by adopting the optimal number of elements in the case 2 ($\mu_1/\mu_0 = 0.6$).

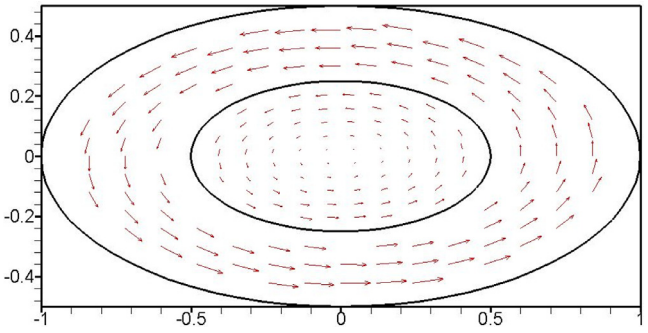

Fig. 37. The field solution of shear flow by adopting the optimal number of elements in the case 2 ($\mu_1/\mu_0 = 0.8$).

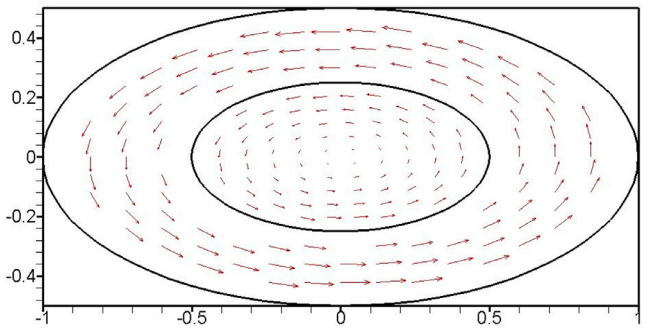

Fig. 38. The field solution of shear flow by adopting the optimal number of elements in the case 2 ($\mu_1/\mu_0 = 1$).

Table 9
Relative error of rigidity for different N_0/N_1 in a circular case with an eccentric inclusion ($\mu_1/\mu_0 = 5$).

N_0/N_1	Relative error of rigidity
1/9	0.15217
1/8	0.12319
1/5	0.06048
1/4	0.04094
1/2	0.01486
1/1	0.00684
2/1	0.00433
4/1	0.00440
5/1	0.00506
8/1	0.00809
9/1	0.00944

Table 10
Relative error of rigidity for different N_0/N_1 in aelliptic case with an elliptic inclusion ($\mu_1/\mu_0 = 0$).

N_0/N_1	Relative error of rigidity
1/9	0.15743
1/8	0.12576
1/5	0.05295
1/4	0.03603
1/2	0.01231
1/1	0.00506
2/1	0.00205
4/1	0.00075
5/1	0.00217
8/1	0.00735
9/1	0.00937

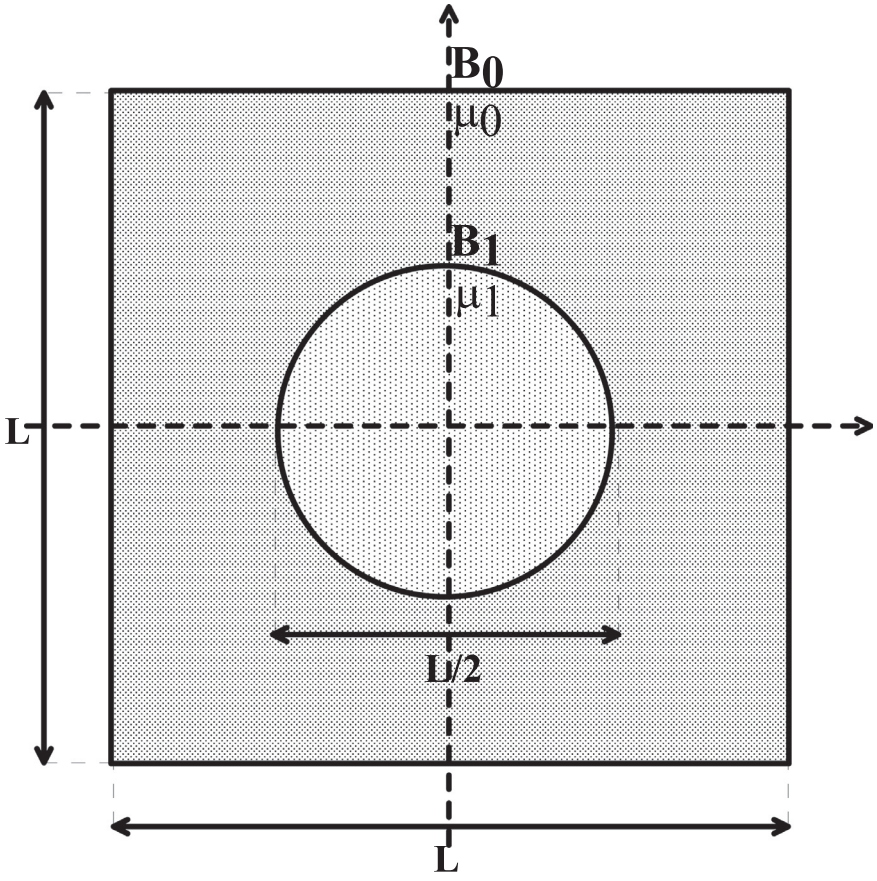

Fig. 39. Sketch of problem in the case 3.

Table 11
Relative error of rigidity for different N_0/N_1 in aelliptic case with an elliptic inclusion ($\mu_1/\mu_0 = 0.2$).

N_0/N_1	Relative error of rigidity
1/9	0.15498
1/8	0.12394
1/5	0.05225
1/4	0.03557
1/2	0.01218
1/1	0.00505
2/1	0.00217
4/1	0.00031
5/1	0.00151
8/1	0.00576
9/1	0.00738

Table 12
Relative error of rigidity for different N_0/N_1 in aelliptic case with an elliptic inclusion ($\mu_1/\mu_0 = 0.4$).

N_0/N_1	Relative error of rigidity
1/9	0.15272
1/8	0.12224
1/5	0.05160
1/4	0.03515
1/2	0.01208
1/1	0.00508
2/1	0.00232
4/1	0.00014
5/1	0.00083
8/1	0.00416
9/1	0.00540

Table 13
Relative error of rigidity for different N_0/N_1 in a elliptic case with an elliptic inclusion ($\mu_1/\mu_0 = 0.6$).

N_0/N_1	Relative error of rigidity
1/9	0.15057
1/8	0.12059
1/5	0.05095
1/4	0.03472
1/2	0.01196
1/1	0.00507
2/1	0.00244
4/1	0.00057
5/1	0.00020
8/1	0.00263
9/1	0.00348

Table 14
Relative error of rigidity for different N_0/N_1 in a elliptic case with an elliptic inclusion ($\mu_1/\mu_0 = 0.8$).

N_0/N_1	Relative error of rigidity
1/9	0.14852
1/8	0.11901
1/5	0.05032
1/4	0.03430
1/2	0.01184
1/1	0.00507
2/1	0.00255
4/1	0.00099
5/1	0.00042
8/1	0.00112
9/1	0.00160

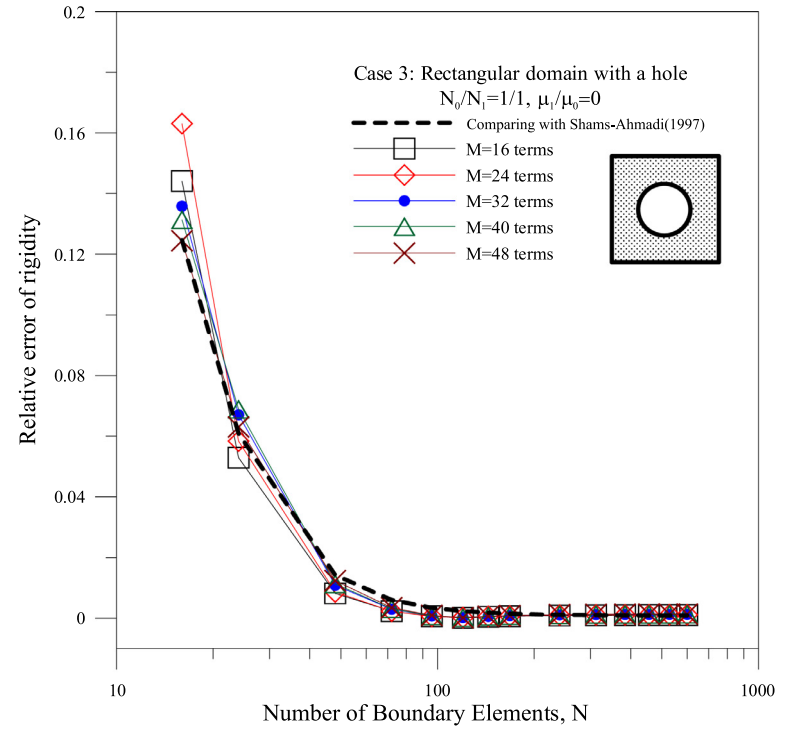

(a) Relative error of rigidity

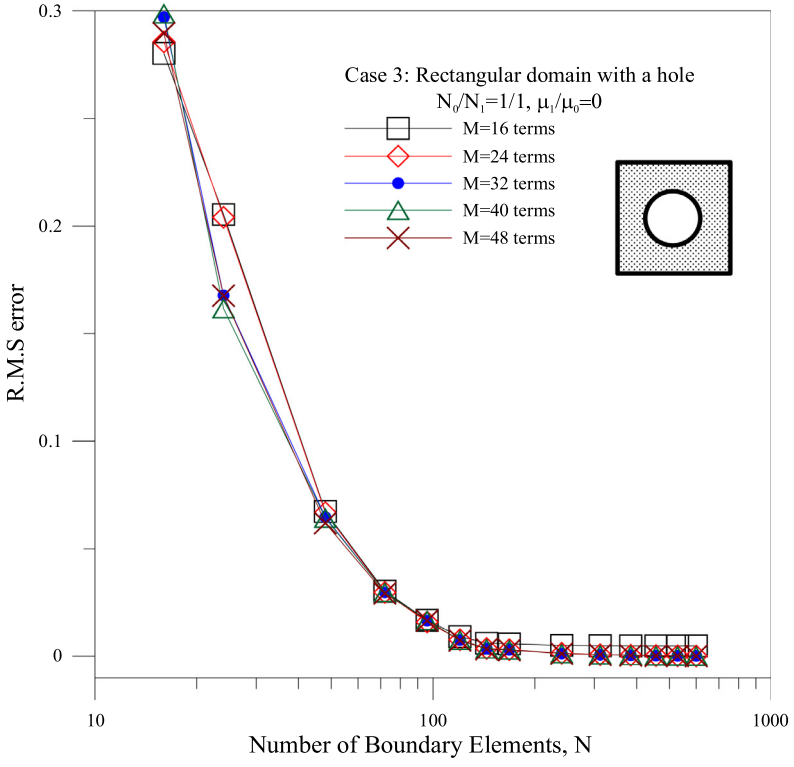

(b) R.M.S error

Fig. 40. The error analysis versus the number of boundary elements for the different terms of Trefftz basis in the case 3 ($\mu_1/\mu_0 = 0$).

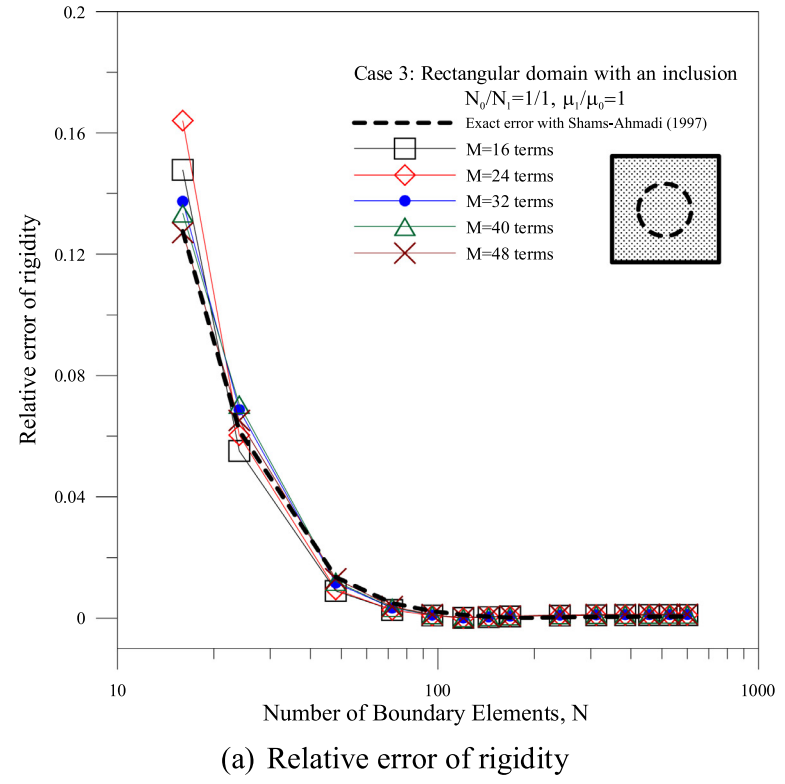

(a) Relative error of rigidity

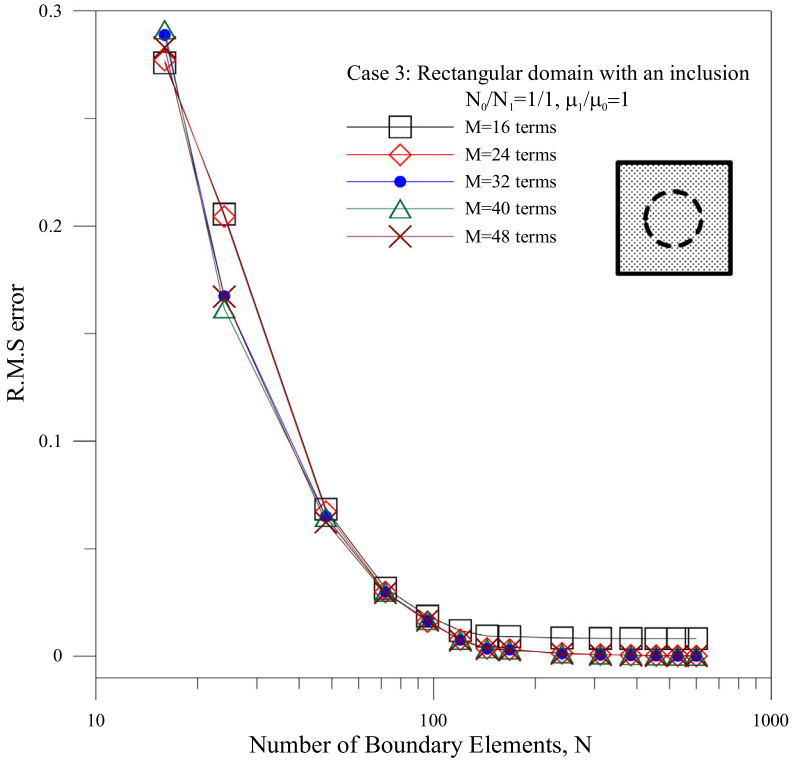

(b) R.M.S error

Fig. 41. The error analysis versus the number of boundary elements for the different terms of Trefftz basis in the case 3 ($\mu_1/\mu_0 = 1$).

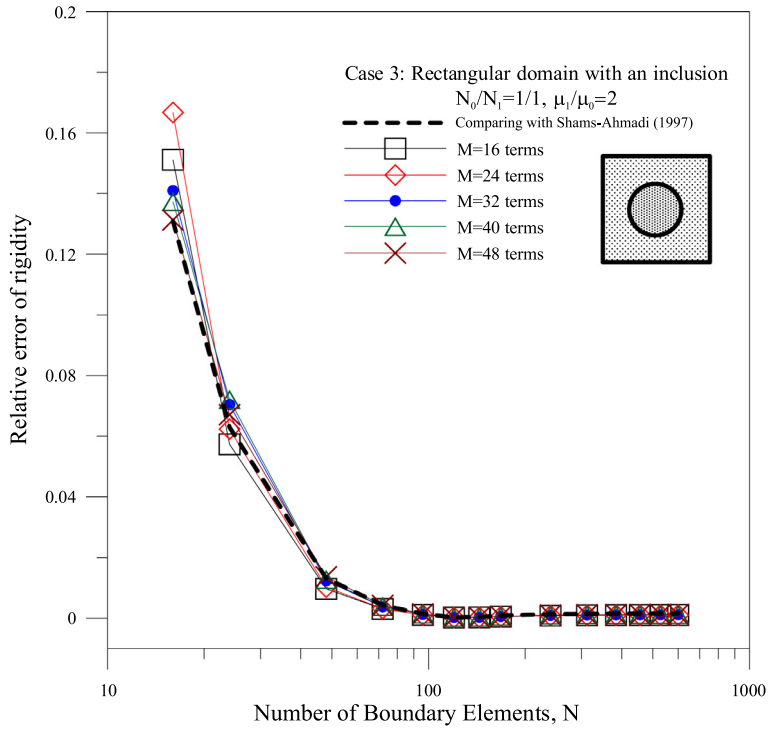

(a) Relative error of rigidity

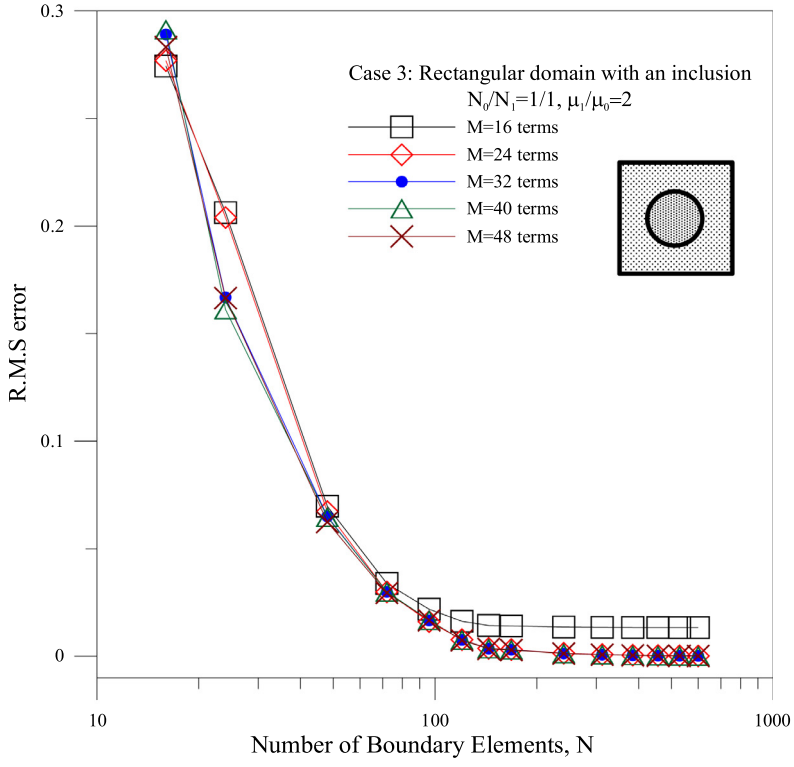

(b) R.M.S error

Fig. 42. The error analysis versus the number of boundary elements for the different terms of Trefftz basis in the case 3 ($\mu_1/\mu_0 = 2$).

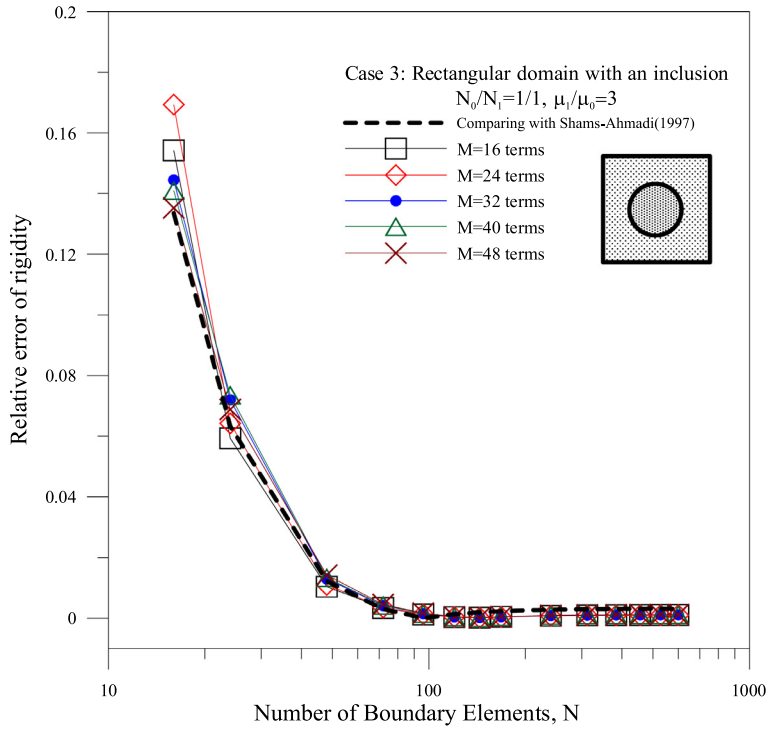

(a) Relative error of rigidity

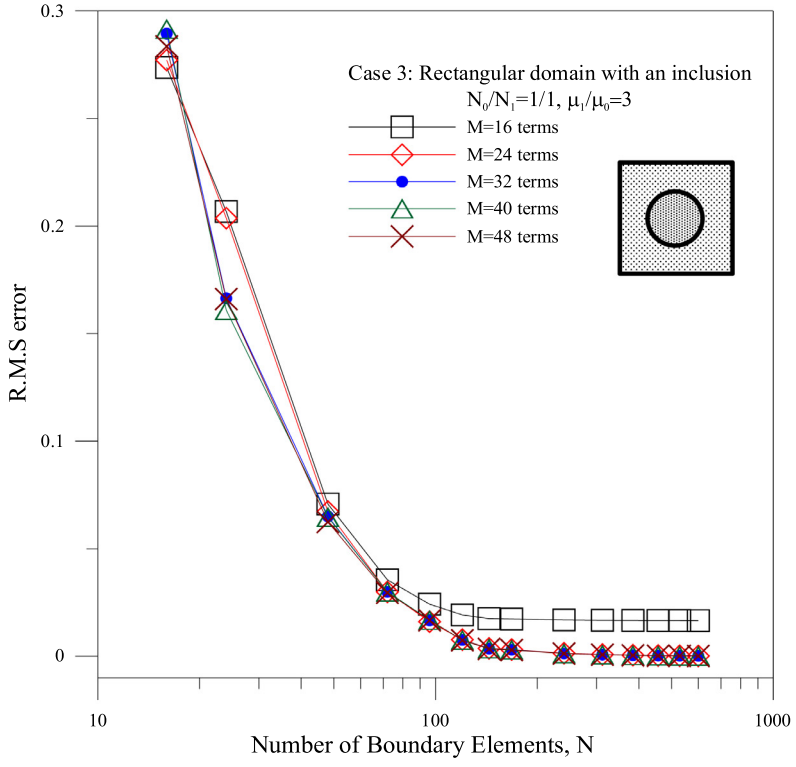

(b) R.M.S error

Fig. 43. The error analysis versus the number of boundary elements for the different terms of Trefftz basis in the case 3 ($\mu_1/\mu_0 = 3$).

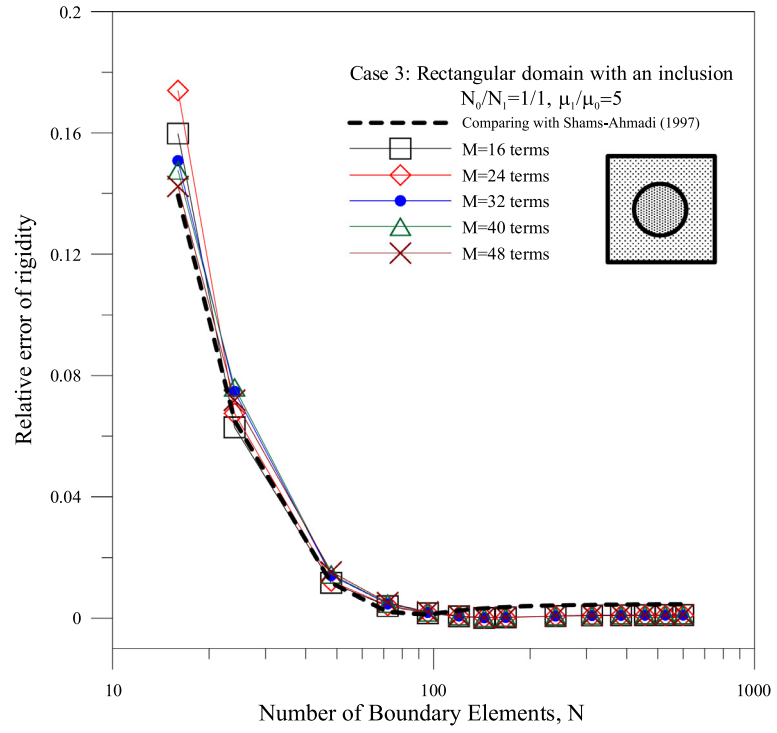

(a) Relative error of rigidity

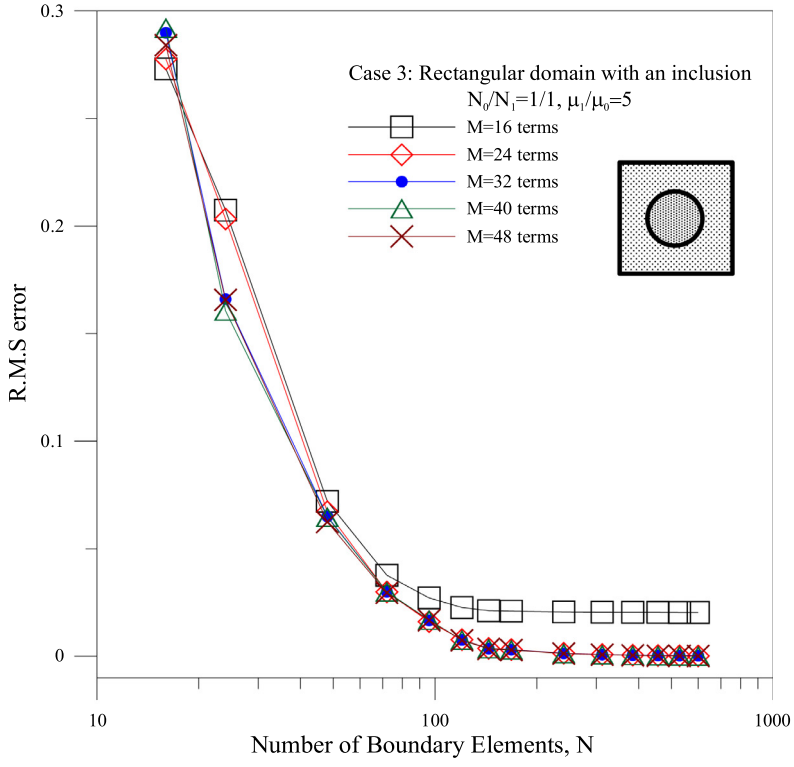

(b) R.M.S error

Fig. 44. The error analysis versus the number of boundary elements for the different terms of Trefftz basis in the case 3 ($\mu_1/\mu_0 = 5$).

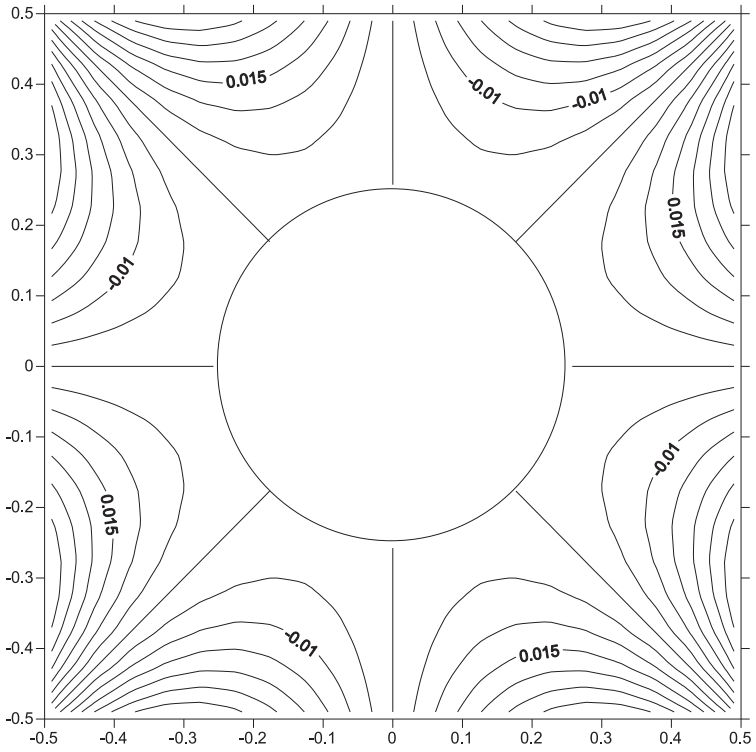

(a) Exact solution of the auxiliary problem (M=48)

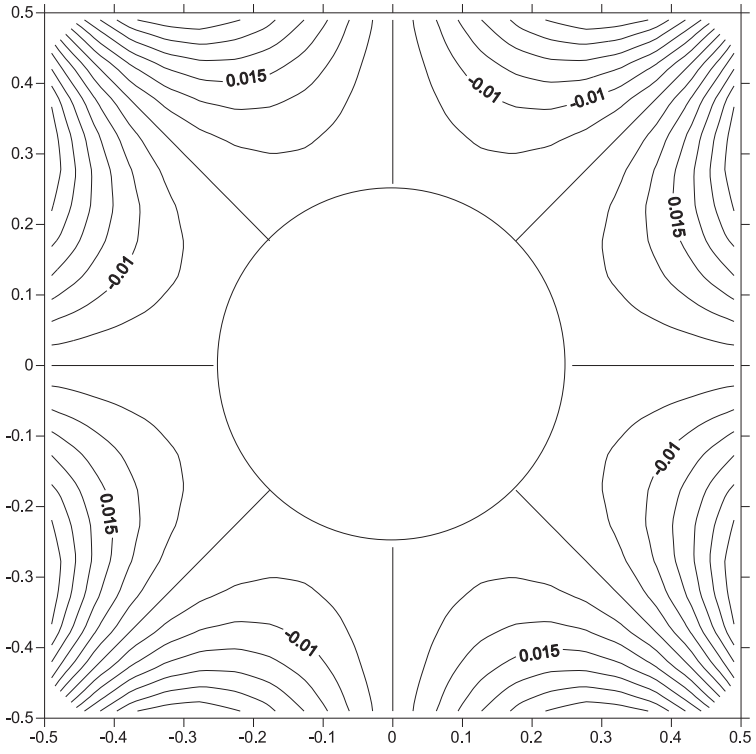

(b) Optimal solution of the original problem (N=96)

Fig. 45. The field solution of warping function in the case 3 ($\mu_1/\mu_0 = 0$).

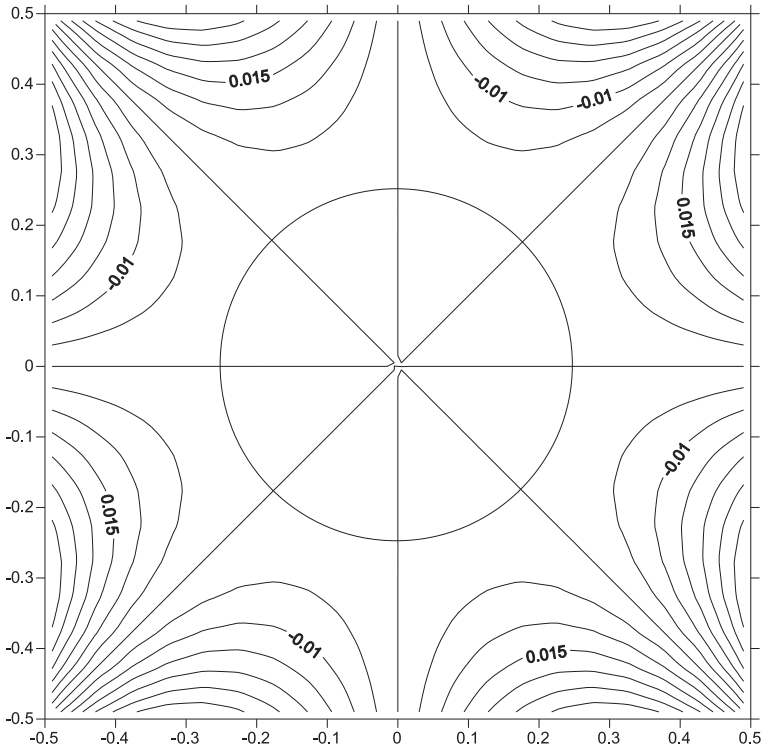

(a) Exact solution of the auxiliary problem (M=48)

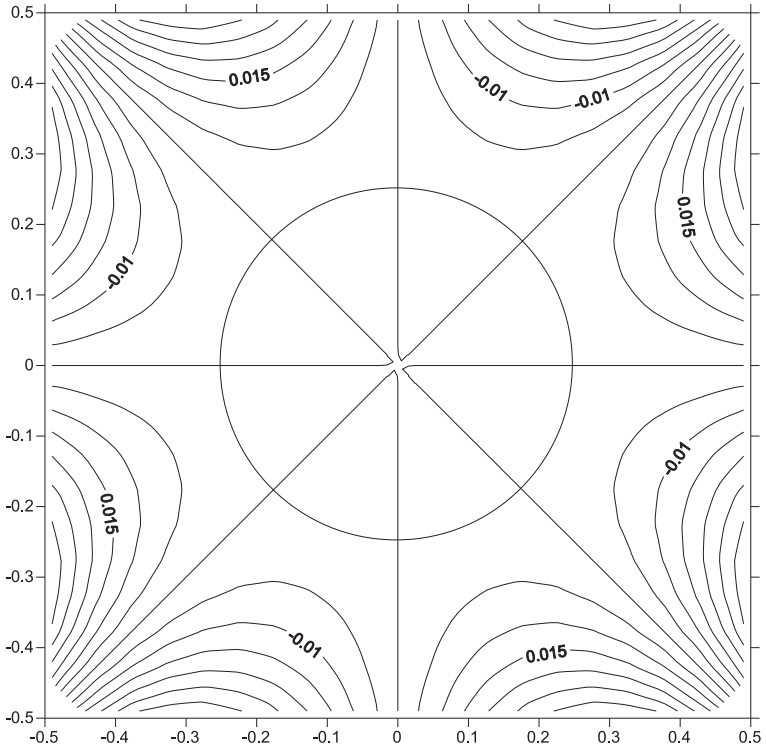

(b) Optimal solution of the original problem (N=96)

Fig. 46. The field solution of warping function in the case 3 ($\mu_1/\mu_0 = 1$).

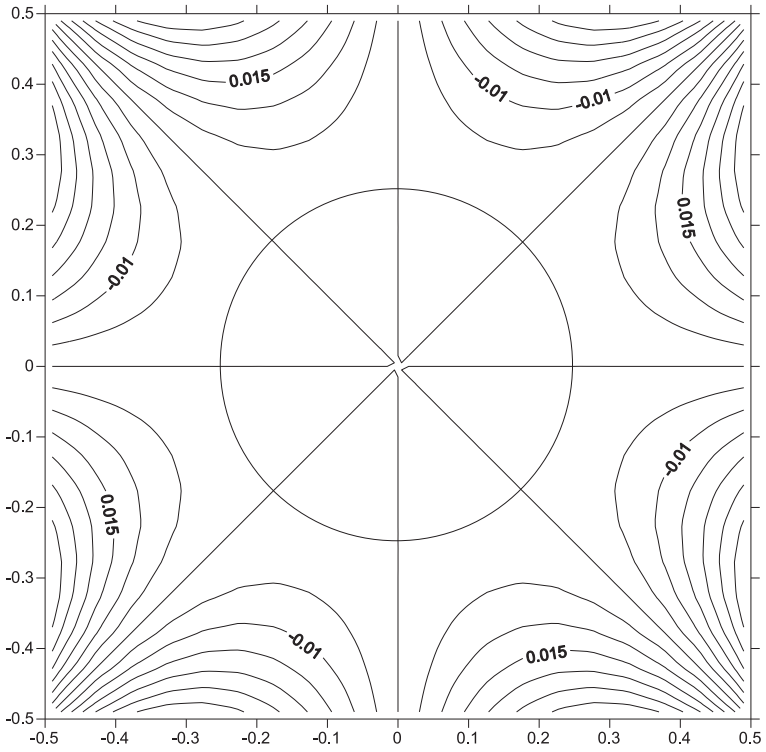

(a) Exact solution of the auxiliary problem (M=48)

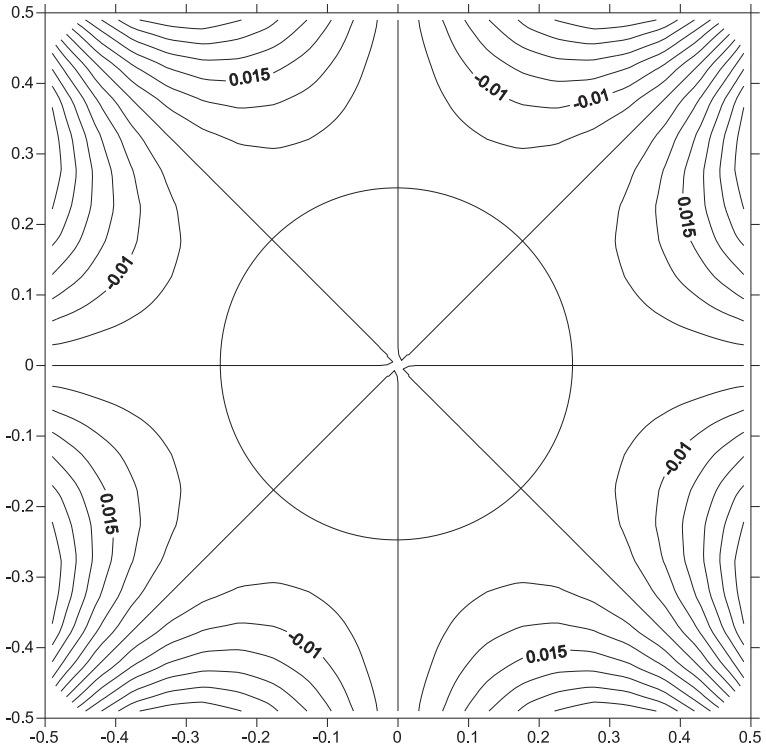

(b) Optimal solution of the original problem (N=96)

Fig. 47. The field solution of warping function in the case 3 ($\mu_1/\mu_0 = 2$).

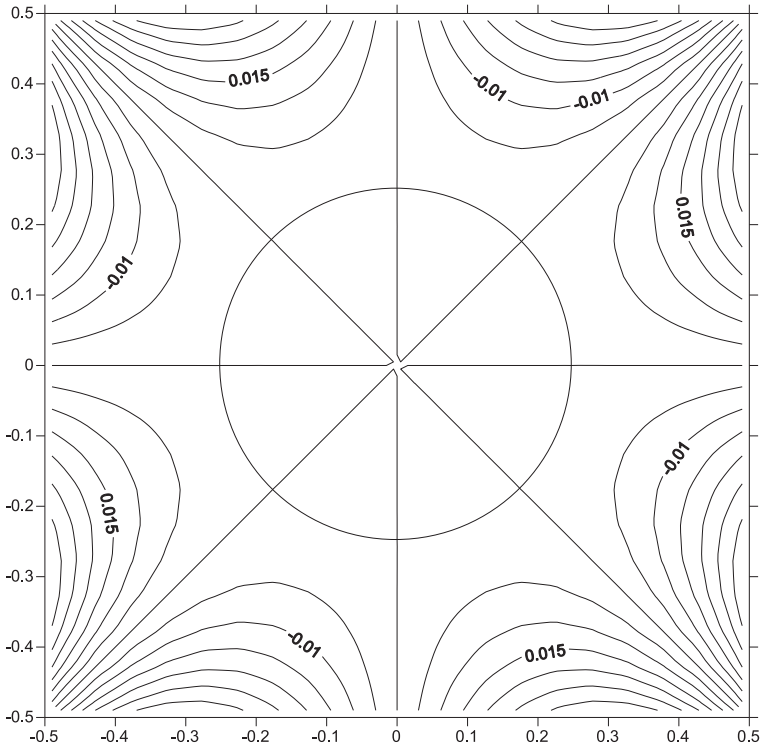

(a) Exact solution of the auxiliary problem (M=48)

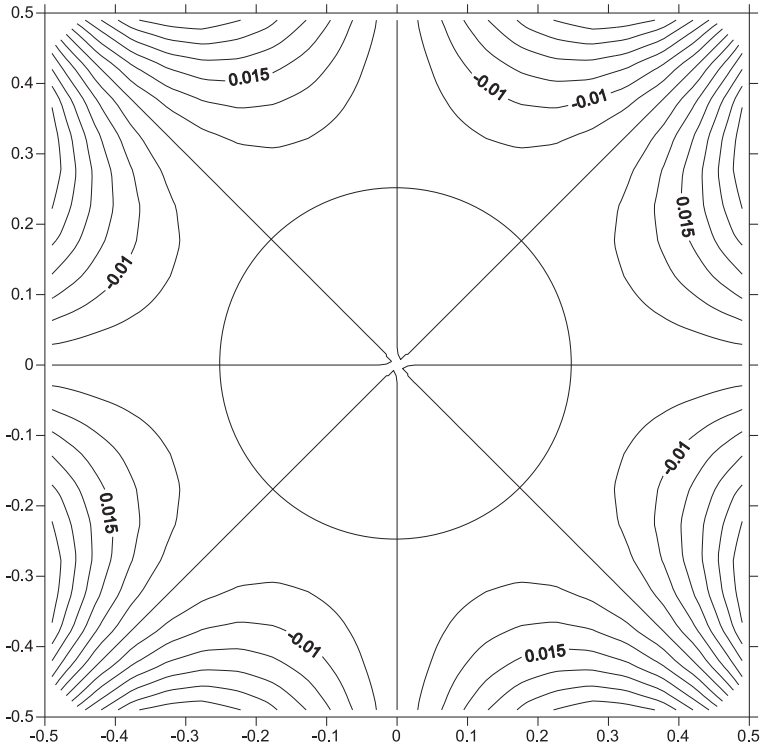

(b) Optimal solution of the original problem (N=96)

Fig. 48. The field solution of warping function in the case 3 ($\mu_1/\mu_0 = 3$).

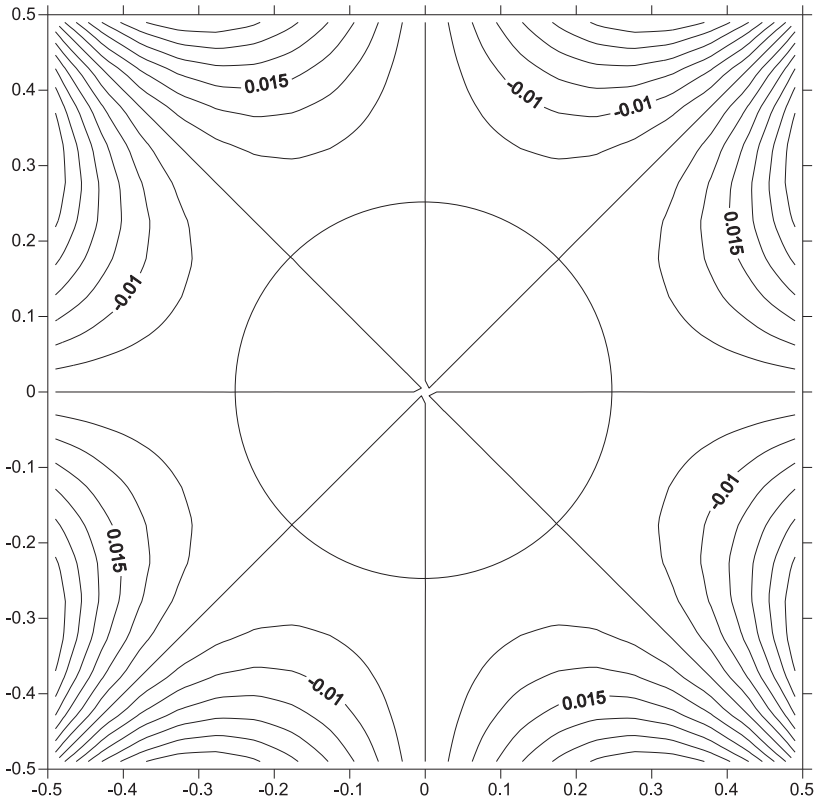

(a) Exact solution of the auxiliary problem (M=48)

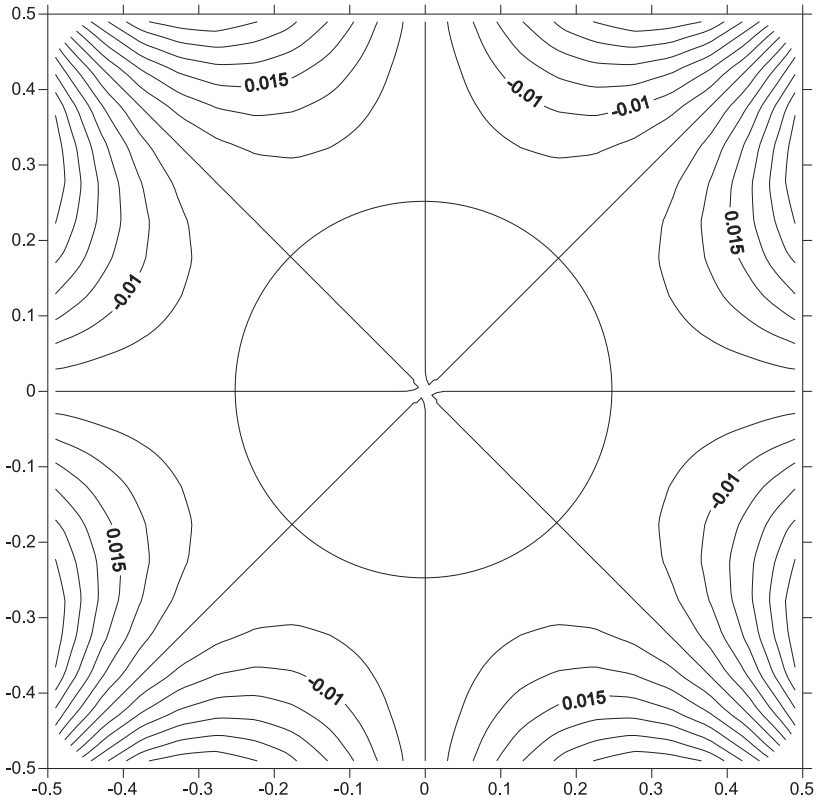

(b) Optimal solution of the original problem (N=96)

Fig. 49. The field solution of warping function in the case 3 ($\mu_1/\mu_0 = 5$).

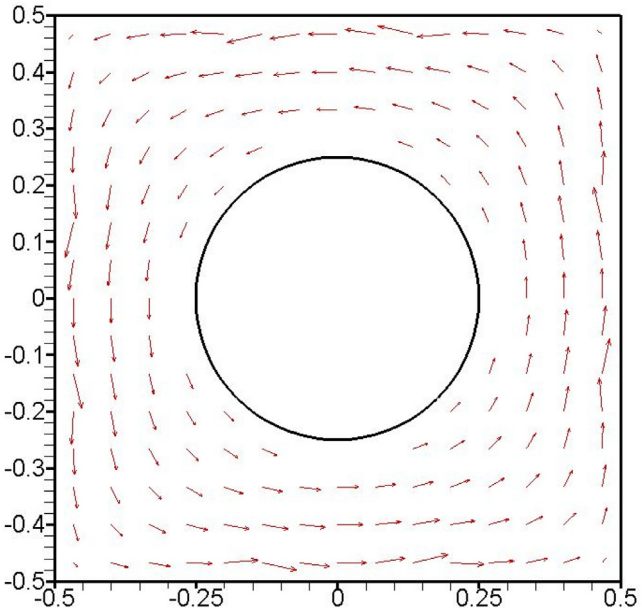

Fig. 50. The field solution of shear flow by adopting the optimal number of elements in the case 3 ($\mu_1/\mu_0 = 0$).

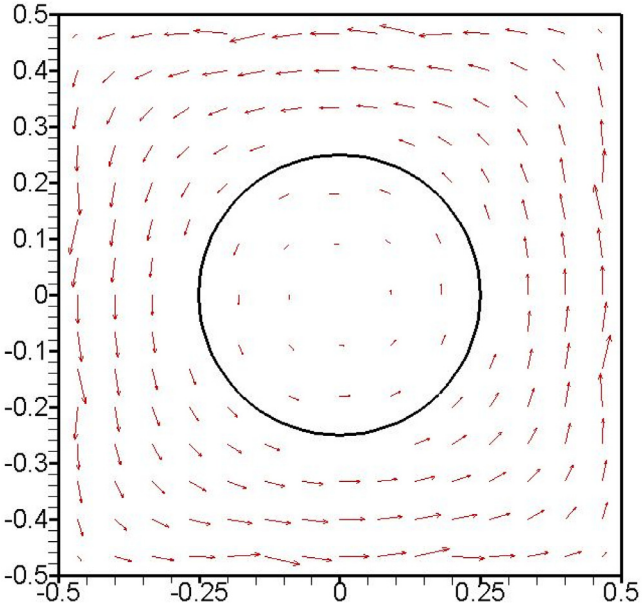

Fig. 51. The field solution of shear flow by adopting the optimal number of elements in the case 3 ($\mu_1/\mu_0 = 1$).

Table 15
Relative error of rigidity for different N_0/N_1 in a elliptic case with an elliptic inclusion ($\mu_1/\mu_0 = 1$).

N_0/N_1	Relative error of rigidity
1/9	0.14656
1/8	0.11748
1/5	0.04971
1/4	0.03389
1/2	0.01173
1/1	0.00507
2/1	0.00267
4/1	0.00140
5/1	0.00103
8/1	0.00034
9/1	0.00024

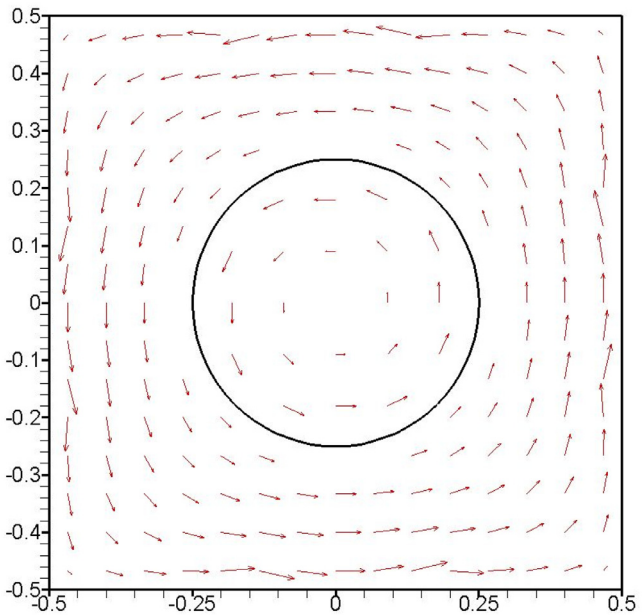

Fig. 52. The field solution of shear flow by adopting the optimal number of elements in the case 3 ($\mu_1/\mu_0 = 2$).

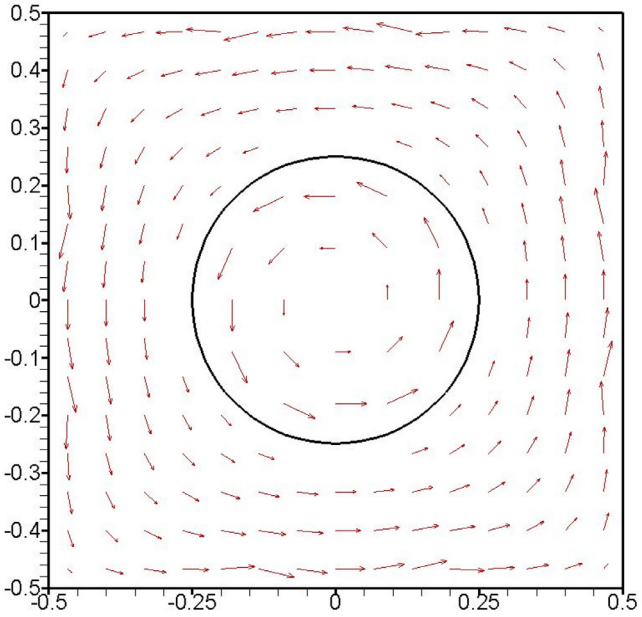

Fig. 53. The field solution of shear flow by adopting the optimal number of elements in the case 3 ($\mu_1/\mu_0 = 3$).

Table 16
Relative error of rigidity for different N_0/N_1 in the rectangular case with a circular inclusion ($\mu_1/\mu_0 = 0$).

N_0/N_1	Relative error of rigidity
1/7	0.06396
1/5	0.03486
1/3	0.01344
1/2	0.00626
1/1	0.00145
2/1	0.00039
3/1	0.00132
5/1	0.00316
7/1	0.00541

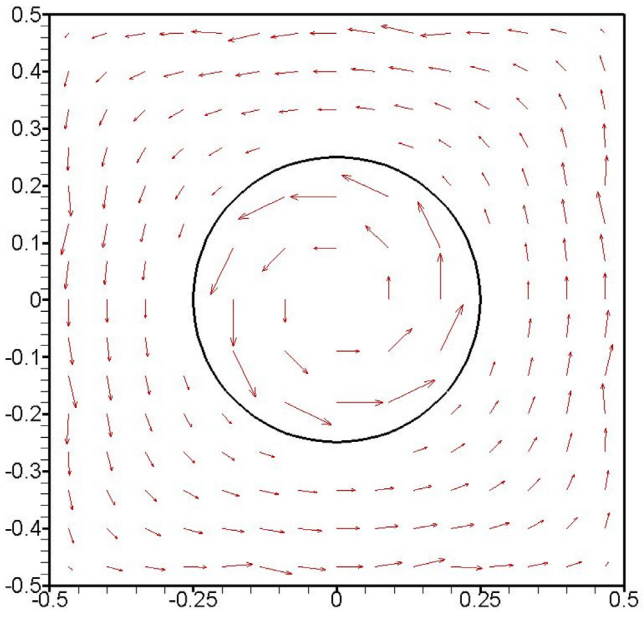

Fig. 54. The field solution of shear flow by adopting the optimal number of elements in the case 3 ($\mu_1/\mu_0 = 5$).

Table 17
Relative error of rigidity for different N_0/N_1 in the rectangular case with a circular inclusion ($\mu_1/\mu_0 = 1$).

N_0/N_1	Relative error of rigidity
1/7	0.06135
1/5	0.03343
1/3	0.01297
1/2	0.00614
1/1	0.00168
2/1	0.00029
3/1	0.00005
5/1	0.00029
7/1	0.00037

Table 18
Relative error of rigidity for different N_0/N_1 in the rectangular case with a circular inclusion ($\mu_1/\mu_0 = 2$).

N_0/N_1	Relative error of rigidity
1/7	0.05890
1/5	0.03213
1/3	0.01255
1/2	0.00604
1/1	0.00189
2/1	0.00094
3/1	0.00112
5/1	0.00234
7/1	0.00422

Conclusions

In order to obtain the optimal solution by adopting various lengths of elements on different boundaries, we employ different configurations of the distribution of the number of elements on the boundaries using the error technique. For the above cases of each μ_1/μ_0, we can obtain the relative error of rigidity with different ratios of exterior and interior elements, respectively. The feasibility for our method can be verified through three numerical cases. We can obtain better results by using our method.

Table 19
Relative error of rigidity for different N_0/N_1 in the rectangular case with a circular inclusion ($\mu_1/\mu_0 = 3$).

N_0/N_1	Relative error of rigidity
1/7	0.05664
1/5	0.03093
1/3	0.01217
1/2	0.00595
1/1	0.00209
2/1	0.00153
3/1	0.00221
5/1	0.00476
7/1	0.00844

Table 20
Relative error of rigidity for different N_0/N_1 in the rectangular case with a circular inclusion ($\mu_1/\mu_0 = 5$).

N_0/N_1	Relative error of rigidity
1/7	0.05260
1/5	0.02881
1/3	0.01148
1/2	0.00579
1/1	0.00245
2/1	0.00259
3/1	0.00413
5/1	0.00906
7/1	0.01592

Acknowledgment

The authors are grateful to the Ministry of Science and Technology of Taiwan for financial support (grant number MOST-07-2221-E-197-008-)

References

[1] Chen KH, Chen JT. Estimating the optimum number of boundary elements by error estimation in a defined auxiliary problem. Eng Anal Bound Elem 2014;39:15–22.
[2] Abbaszadeh M, Dehghan M. The reproducing kernel particle Petrov–Galerkin method for solving two-dimensional nonstationary incompressible Boussinesq equations. Eng Anal Bound Elem 2019;106:300–8.
[3] Abbaszadeh M, Khodadadian A, Parvizi M, Dehghan M, Heitzinger C. A direct meshless local collocation method for solving stochastic Cahn-Hilliard-Cook and stochastic Swift-Hohenberg equations. Eng Anal Bound Elem 2019;98:253–64.
[4] Dehghan M, Abbaszadeh M. Error analysis and numerical simulation of magneto-hydrodynamics (MHD) equation based on the interpolating element free Galerkin (IEFG) method. Appl Numer Math 2019;137:252–73.
[5] Liu CS. A highly accurate collocation trefftz method for solving the Laplace equation in the doubly connected domains. Numer Methods Partial Differ Equ 2008;24:179–92.
[6] Chen JT, Kao SK, Lee WM, Lee YT. Eigensolutions of the Helmholtz equation for a multiply connected domain with circular boundaries using the multipole Trefftz method. Eng Anal Bound Elem 2010;34(5):463–70.
[7] Chen KH, Chen JT, Chou CR, Yueh CY. Dual boundary element analysis of oblique incident wave passing a thin submerged breakwater. Eng Anal Bound Elem 2002;26:917–28.
[8] Chen H, Jin J, Zhang P, Pin L. Multi-Variable non-singular BEM for 2-D potential problems. Tsinghua Sci Technol 2005;10:43–50.
[9] Golberg MA, Bowman H. Super convergence and the use of the residual as an error estimator in the BEM. Eng Anal Bound Elem 1999;25:511–21.
[10] Huang CS, Lee CF, Cheng AHD. Error estimate, optimal shape factor, and high precision computation of multiquadric collocation method. Eng Anal Bound Elem 2007;31:614–23.
[11] Liang MT, Chen JT, Yang SS. Error estimation for boundary element method. Eng Anal Bound Elem 1999;23:257–65.

[12] Vable M. Controlling errors in the process of automating boundary element method analysis. Eng Anal Bound Elem 2002;26:405–15.
[13] Zhao Z, Wang X. Error estimation and h adaptive boundary elements. Eng Anal Bound Elem 1999;23:793–803.
[14] Muskhelishvili NI. Some basic problems of the mathematical theory of elasticity. Springer; 1953.
[15] Sapountzakis EJ, Mokos VG. Warping shear stresses in nonuniform torsion of composite bars by BEM. Comput Method Appl Mech Eng 2003;192:4337–53.
[16] Timoshenko SP, Gooder JN. Theory of elasticity. McGraw-Hill; 1970.
[17] Katsikadelis JT, Sapountzakis EJ. Torsion of composite bars by boundary element method. ASCE J Eng Mech 1985;111:1197–210.
[18] Shams-Ahmadi M, Chou SI. Complex variable boundary element method for torsion of composite shafts. Int J Numer Meth Eng 1997;40:1165–79.
[19] Chen JT, Chen KH, Yeih W, Shieh NC. Dual boundary element analysis for cracked bars under torsion. Eng Comput 1998;Vol.15:732–49.
[20] Jhong FL. Application of new error estimation technique to the method of fundamental solutions and Trefftz method for solving the boundary value problem of Helmholtz equation Master thesis. National Ilan University; 2011.
[21] Chen JT, Lee YT. Torsional rigidity of a circular bar with multiple circular inclusions using a null field integral equations. Comput Mech 2009;44:221–32.